

A C^1 -conforming arbitrary-order two-dimensional virtual element method for the fourth-order phase-field equation

Dibyendu Adak^a, Gianmarco Manzini^{b,*}, Hashem M. Mourad^c, JeeYeon N. Plohr^d, Lampros Svolos^c

^a*GIMNAP, Departamento de Matemática, Universidad del Bío-Bío, Concepción, Chile*

^b*Applied Mathematics and Plasma Physics, T-5, Theoretical Division, Los Alamos National Laboratory, Los Alamos, NM, USA*

^c*Fluid Dynamics and Solid Mechanics, T-3, Theoretical Division, Los Alamos National Laboratory, Los Alamos, NM, USA*

^d*Materials and Physical Data, XCP-5, Computational Physics Division, Los Alamos National Laboratory, Los Alamos, NM, USA*

Abstract

We present a two-dimensional conforming virtual element method for the fourth-order phase-field equation. Our proposed numerical approach to the solution of this high-order phase-field (HOPF) equation relies on the design of an arbitrary-order accurate, virtual element space with C^1 global regularity. Such regularity is guaranteed by taking the values of the virtual element functions and their full gradient at the mesh vertices as degrees of freedom. Attaining high-order accuracy requires also edge polynomial moments of the trace of the virtual element functions and their normal derivatives. In this work, we detail the scheme construction, and prove its convergence by deriving error estimates in different norms. A set of representative test cases allows us to assess the behavior of the method.

Keywords: Two-dimensional phase field equation, virtual element method, error analysis.

2020 Mathematics Subject Classification: Primary: 65M60, 65N30; Secondary: 65M22.

1. Introduction

Fracture is a critical failure mode that can cause a rapid loss of load-carrying capacity and uncontrolled demolition of inhabited structures. The prevention of such catastrophic outcomes is the motivation to develop computationally efficient models of fracture, which are also capable of accurately capturing material behavior in the post-failure regime. The efficient solution to fracture problems remains one of the most critical research priorities despite the progress made over the past decades. To this end, developing efficient numerical techniques with predictive capabilities requires a multidisciplinary approach.

Over the past decade, phase field (PF) modeling of fracture has gained significant attention due to its ability to capture complicated crack patterns (e.g., merging or branching) by utilizing conventional finite element techniques. The first PF fracture method is traced back to Bourdin et al. [18], where a numerical implementation of the variational approach to fracture [27] was introduced. Inspired by Griffith's work, the variational approach describes fracture as a minimization problem of a total energy functional, which expresses the competition between bulk elastic energy and crack surface energy. By introducing an auxiliary field (denoted by u in this paper), crack surfaces are represented by "diffuse" entities, obviating the need for injecting discontinuities into the kinematic solution fields. In the seminal work of Miehe et al. [35], a framework based on continuum mechanics and thermodynamic arguments was proposed to model brittle fracture. It was further developed to treat dynamic brittle failure in [17].

*Corresponding author

Email address: gmanzini@lanl.gov (Gianmarco Manzini)

Moreover, the PF framework was extended to model cohesive fracture in [44] and ductile fracture in [34]. More recently, multiphysics coupling effects are studied in problems of brittle fracture [46], cohesive fracture [38], ductile fracture [24, 41, 42], and structural fragmentation [36]. The interested reader is referred to [25, 37] for more applications of the PF method and to [45] for an extensive review.

The numerical solution to PF fracture problems may require a highly refined mesh to accurately resolve the steep PF gradients that develop in the vicinity of a crack [45], thus being expensive and possibly non-competitive with respect to other approaches despite all its modeling capabilities. Adopting the popular second-order PF fracture model exacerbates this issue, as it leads to the development of a cusp in the solution field at the crack surface that negatively impacts the convergence of the numerical solution when the mesh is refined. To address this issue, Borden et al. [16] proposed a high-order phase-field (HOPF) model, where the solution regularity is increased, and better spatial convergence behavior can be achieved. The HOPF model involves a trade-off, as it necessitates using specialized computational techniques that ensure C^1 -continuity of the PF unknown to attain convergence. For example, the Finite Element Method (FEM) with a C^0 -continuous Lagrange polynomial basis is not a good choice. Its use to treat higher-order PF problems results in discontinuities in the PF gradient. Thus, it constitutes a variational crime [40], since the weak form of such problems includes at least second-order spatial derivatives, e.g., the Laplacian and the Hessian differential operators.

High regularity of the numerical approximation is of primary importance when dealing with high-order differential problems. In addition, global smoothness can be utilized to directly compute physical quantities (such as fluxes, strains, and stresses) without resorting to post-processing as in the C^0 -FEM. From the earliest works in the 1960s, e.g., [7, 14], to the most current attempts, e.g., [32, 47], there are several examples of finite elements with regularity higher than C^0 . The construction of approximation spaces with such global regularity has been seen as challenging since they require basis functions with the same global regularity. Designing approximations with such enhanced regularity is still an active research topic. A non-exhaustive list includes the FEM with Hermite polynomial basis functions [39] or B-spline basis functions (i.e., isogeometric analysis) [9]; machine learning techniques (e.g. physics informed neural networks [29]); fast Fourier transform (FFT)-based methods [33]; mixed FEM [26]; continuous/discontinuous Galerkin (C/DG) methods [43]; discontinuous Galerkin (DG) methods [28]. Such approximations have a natural application in the numerical treatment of problems involving high-order differential operators, as in the HOPF problem.

The Virtual Element Method (VEM) was initially designed as a Galerkin-type projection method to extend the FEM from triangular/tetrahedral and quadrilateral/hexahedral meshes to polytopal meshes. The VEM does not need explicit knowledge of the basis functions spanning the approximation spaces [10]. Instead, local approximation spaces are constructed by solving a partial differential equation at the element level. These local spaces are subsequently “glued” together to form a highly regular, conforming global approximation space. The basis functions in this case are referred to as “virtual” because they are not computed in closed form. Only the projection of the basis onto a subspace of polynomials is known, and is utilized in the method’s formulation. The conforming VEM was first developed for second-order elliptic problems in primal formulation [10], and then in nonconforming formulation [8]. The first works using a C^1 -regular conforming VEM addressed the classical plate bending problems [20, 22], second-order elliptic problems [12, 13], and the nonlinear Cahn-Hilliard equation [3]. In [6], a highly-regular conforming VEM is proposed for the two-dimensional polyharmonic problem $(-\Delta)^{p_1} u = f$, $p_1 \geq 1$. The VEM is based on an approximation space that locally contains polynomials of degree $r \geq 2p_1 - 1$ and has a global H^{p_1} regularity. In [5], this formulation was extended to a virtual element space that can have arbitrary regularity $p_2 \geq p_1 \geq 1$ and contains polynomials of degree $r \geq p_2$. Highly-regular conforming VEM in any dimension has been proposed in [21].

HOPF models of dynamic fracture are based on two coupled governing equations: the momentum conservation equation and the HOPF evolution equation. In our recent work [4], we developed a VEM for the momentum equation with linear elastic constitutive laws. In the present work, we propose a VEM

for the other ingredient of HOPF fracture models, namely the HOPF evolution equation itself. The coupling between these two virtual element models is a non-trivial task, and will be the topic of our future work. Specifically, we design a conforming VEM for the fourth-order equation with Laplace and L^2 terms. The numerical approximation relies on an arbitrary order accurate, virtual element space with H^2 global regularity. The degrees of freedom of the lowest-order accurate C^1 -VEM are the values of the virtual element functions and their gradients at the mesh vertices. Attaining high-order accuracy requires additional edge polynomial moments of the trace of the virtual element functions and their normal derivatives. This choice of the degrees of freedom guarantees the global H^2 regularity. To avoid the computational complexity of the lower order terms, we introduce an elliptic projection operator that combines the biharmonic and Laplace operators. The calculation of the elliptic projection in every cell reduces to a single matrix calculation instead of two, and our approach requires less computation than the ones proposed in the existing VEM literature. Furthermore, the use of a single elliptic projection simplifies the fixing of the kernel that reduces to the kernel of the Laplacian operator. This technique reduces the computational cost significantly for higher order VEM spaces and, potentially, for higher dimensions.

The remainder of this paper is organized as follows. In Section 2, we briefly discuss the strong and weak formulations of the HOPF model along with the mathematical arguments proving their well-posedness. In Section 3, we construct the virtual element approximation of the HOPF equation through the definition of the virtual element space and the bilinear forms and linear functional required by the variational formulation. In Section 4, we conduct a convergence analysis of the proposed VEM by deriving error estimates of the discrete scheme. In Section 5, we discuss the implementation of the method and provide details on the discretization. In Section 6, we carry out a numerical investigation about the performance of the proposed method by solving a manufactured solution problem on a set of representative polygonal meshes. In addition, we show that optimal convergence rates are attained for an example involving a diagonal crack modeled by the phase-field method. In Section 7, we offer our final conclusions and remarks on possible future work.

1.1. Notation and technicalities

Throughout this paper, we adopt the notation of Sobolev spaces of Ref. [2]. Accordingly, we denote the space of square integrable functions defined on any open, bounded, connected domain $\mathcal{D} \subset \mathbb{R}^2$ with boundary $\partial\mathcal{D}$ by $L^2(\mathcal{D})$, and the Hilbert space of functions in $L^2(\mathcal{D})$ with all partial derivatives up to a positive integer m also in $L^2(\mathcal{D})$ by $H^m(\mathcal{D})$, cf. [2]. We endow $H^m(\mathcal{D})$ with a norm and a seminorm that we denote as $\|\cdot\|_{m,\mathcal{D}}$ and $|\cdot|_{m,\mathcal{D}}$, respectively.

The virtual element method is formulated on the mesh family $\{\Omega_h\}_h$, where each mesh Ω_h is a partition of the computational domain Ω into nonoverlapping polygonal elements E . A polygonal element E is a compact subset of \mathbb{R}^2 with boundary ∂E , area $|E|$, center of gravity \mathbf{x}_E , and diameter $h_E = \sup_{\mathbf{x},\mathbf{y} \in E} |\mathbf{x} - \mathbf{y}|$. The mesh elements of Ω_h form a finite cover of Ω such that $\bar{\Omega} = \cup_{E \in \Omega_h} E$ and the mesh size labeling each mesh Ω_h is defined by $h = \max_{E \in \Omega_h} h_E$. A mesh edge e has center \mathbf{x}_e and length h_e ; a mesh vertex v has position vector \mathbf{x}_v .

We denote the set of mesh edges by \mathcal{E}_h and the set of mesh vertices by \mathcal{V}_h . We decompose the edge set as $\mathcal{E}_h := \mathcal{E}_h^{\text{int}} \cup \mathcal{E}_h^{\text{bdry}}$, where $\mathcal{E}_h^{\text{int}}$ and $\mathcal{E}_h^{\text{bdry}}$ are the set of interior and boundary edges. Similarly, we decompose the vertex set as $\mathcal{V}_h := \mathcal{V}_h^{\text{int}} \cup \mathcal{V}_h^{\text{bdry}}$, where $\mathcal{V}_h^{\text{int}}$ and $\mathcal{V}_h^{\text{bdry}}$ are the set of interior and boundary vertices. For each $E \in \Omega_h$, we denote by \mathbf{n}_E the unit normal vector and by \mathbf{t}_E the unit tangential vector along the boundary ∂E . We assume a local orientation of ∂E so that \mathbf{n}_E point out of E . Besides, we will use $\mathbf{n}_{E,e}$ and $\mathbf{t}_{E,e}$ to denote the unit normal and tangential vectors to an edge $e \in \mathcal{E}_h$ that are locally oriented consistently with ∂E and \mathbf{n}_e and \mathbf{t}_e the vectors whose orientation is globally fixed once and for all (and independent of ∂E). Moreover, in the definition of the degrees of freedom of the next section, we also associate every vertex v with a characteristic length h_v , which is the average of the diameters of the polygons sharing that vertex.

For any integer number $\ell \geq 0$, we let $\mathbb{P}_\ell(\mathbf{E})$ and $\mathbb{P}_\ell(\mathbf{e})$ denote the space of polynomials defined on the element \mathbf{E} and the edge \mathbf{e} , respectively; $\mathbb{P}_\ell(\Omega_h)$ denotes the space of piecewise polynomials of degree ℓ on the mesh Ω_h . For convenience of exposition, we also use the notation $\mathbb{P}_{-2}(\mathbf{E}) = \mathbb{P}_{-1}(\mathbf{E}) = \{0\}$. Accordingly, it holds that $q|_{\mathbf{E}} \in \mathbb{P}_\ell(\mathbf{E})$ if $\mathbf{E} \in \Omega_h$ for all $q \in \mathbb{P}_\ell(\Omega_h)$. Finally, we define the (broken) seminorm of a function $v \in \prod_{\mathbf{E} \in \Omega_h} H^2(\mathbf{E})$ by

$$\|v\|_h^2 = \sum_{\mathbf{E} \in \Omega_h} a^{\mathbf{E}}(v, v).$$

Throughout the paper, we use the multi-index notation, so that $\nu = (\nu_1, \nu_2)$ is a two-dimensional index defined by the two integer numbers $\nu_1, \nu_2 \geq 0$. Moreover, $D^\nu w = \partial^{|\nu|} w / \partial x_1^{\nu_1} \partial x_2^{\nu_2}$ denotes the partial derivative of order $|\nu| = \nu_1 + \nu_2 > 0$ of a sufficiently regular function $w(x_1, x_2)$, and we use the conventional notation that $D^{(0,0)} w = w$ for $\nu = (0, 0)$. We also denote the partial derivatives of w versus x and y by the shortcuts $\partial_x w$ and $\partial_y w$, and the normal and tangential derivatives with respect to a given edge by $\partial_n w$ and $\partial_t w$.

2. The high-order phase-field model

Let $\Omega \subset \mathbb{R}^2$ be a simply-connected, open, bounded domain with polygonal boundary Γ . The HOPF model is given by the linear, fourth-order, partial differential equation problem for the real, scalar unknown u :

$$\alpha_2 \Delta^2 u - \alpha_1 \Delta u + \alpha_0 u = f \quad \text{in } \Omega, \quad (1a)$$

$$u = g_0 \quad \text{on } \Gamma, \quad (1b)$$

$$\partial_n u = g_1 \quad \text{on } \Gamma, \quad (1c)$$

where α_0, α_1 and α_2 are strictly-positive, real constant coefficients; $f \in L^2(\Omega)$ is the load term; $g_0 \in H^{\frac{3}{2}}(\Gamma)$ and $g_1 \in H^{\frac{1}{2}}(\Gamma)$ are the univariate functions defining the Dirichlet boundary conditions on Γ .

Consider the affine space $V = \{v \in H^2(\Omega), v|_\Gamma = g_0, \partial_n v|_\Gamma = g_1\}$, and its linear subspace $V_0 = H_0^2(\Omega)$, which we equivalently define by setting $g_0 = g_1 = 0$ in V . The weak formulation of problem (1) reads as:

$$\text{Find } u \in V_0 \text{ such that } \mathcal{A}(u, v) = F(v) \quad \forall v \in V_0, \quad (2)$$

where the bilinear form $\mathcal{A} : V_0 \times V_0 \rightarrow \mathbb{R}$ and the linear functional $F : V_0 \rightarrow \mathbb{R}$ are defined as follows:

$$\mathcal{A}(u, v) := \alpha_2 \mathcal{A}_2(u, v) + \alpha_1 \mathcal{A}_1(u, v) + \alpha_0 \mathcal{A}_0(u, v), \quad (3)$$

with

$$\mathcal{A}_2(u, v) := \int_\Omega \Delta u \Delta v \, d\mathbf{x}, \quad \mathcal{A}_1(u, v) := \int_\Omega \nabla u \cdot \nabla v \, d\mathbf{x}, \quad \mathcal{A}_0(u, v) := \int_\Omega u v \, d\mathbf{x}, \quad (4)$$

and

$$F(v) := \int_\Omega f v \, d\mathbf{x}.$$

For the exposition's convenience, we will also use the additional bilinear form $\mathcal{B} : V_0 \times V_0 \rightarrow \mathbb{R}$ given by $\mathcal{B}(u, v) := \alpha_2 \mathcal{A}_2(u, v) + \alpha_1 \mathcal{A}_1(u, v)$, which is clearly such that $\mathcal{A}(u, v) = \mathcal{B}(u, v) + \alpha_0 \mathcal{A}_0(u, v)$. The positive sublinear functional $\|\cdot\|_{V_0} : V_0 \rightarrow \mathbb{R}^+$ given by

$$\|v\|_{V_0}^2 = \int_\Omega (|\Delta v|^2 + |\nabla v|^2 + |v|^2) \, d\mathbf{x} \quad (5)$$

is a norm on V_0 , and it trivially holds that $\|v\|_{V_0} \leq 2\|v\|_{2,\Omega}$. The bilinear form $\mathcal{A}(\cdot, \cdot)$ is coercive with respect to the norm $\|\cdot\|_{V_0}$. The coercivity of $\mathcal{A}(\cdot, \cdot)$ with coercivity constant $\alpha = \min(\alpha_0, \alpha_1, \alpha_2)$ follows on noting that

$$\mathcal{A}(v, v) \geq \min(\alpha_0, \alpha_1, \alpha_2) \int_{\Omega} (|\Delta v|^2 + |\nabla v|^2 + |v|^2) d\mathbf{x} = \min(\alpha_0, \alpha_1, \alpha_2) \|v\|_{V_0}^2, \quad (6)$$

since $\min(\alpha_0, \alpha_1, \alpha_2) > 0$.

The symmetric bilinear form $\mathcal{A}(\cdot, \cdot)$ is an inner product on $H^2(\Omega)$ since from the coercivity of $\mathcal{A}(\cdot, \cdot)$ it follows that $\mathcal{A}(v, v) = 0$ implies that $v = 0$. The Cauchy-Schwarz inequality implies an upper bound for $\mathcal{A}(u, v)$ with continuity constant equal to $\max(\alpha_0, \alpha_1, \alpha_2)$,

$$\mathcal{A}(v, v) \leq \max(\alpha_0, \alpha_1, \alpha_2) \int_{\Omega} (|\Delta v|^2 + |\nabla v|^2 + |v|^2) d\mathbf{x} = \max(\alpha_0, \alpha_1, \alpha_2) \|v\|_{V_0}^2. \quad (7)$$

The well-posedness follows from an application of the Lax-Milgram theorem since $\mathcal{A}(\cdot, \cdot)$ is coercive and continuous and $F(\cdot)$ is continuous [19].

3. Virtual element approximation of the HOPF problem

The virtual element method that approximates the variational formulation (2) reads as

$$\text{Find } u_h \in V_k^h \text{ such that } \mathcal{A}_h(u_h, v_h) = \langle f_h, v_h \rangle \quad \forall v_h \in V_k^h. \quad (8)$$

In this formulation, V_k^h is the H^2 -conforming approximation of the space $H^2(\Omega)$ provided by the VEM, u_h and v_h are the trial and test functions from this space, and $f_h \in (V_k^h)'$ is a linear operator in the dual space $(V_k^h)'$ that approximates the load term f . We define all these mathematical entities in the rest of this section, which we devote to the construction of the VEM.

3.1. Local enlarged virtual element space, functionals and the elliptic projector $\Pi_k^{\mathcal{L},E}$

Consider the space of functions on the polygonal boundary ∂E for all integer $k \geq 2$ given by

$$B_k^h(\partial E) := \left\{ v_h \in C^1(\partial E) \text{ such that } v_h|_e \in \mathbb{P}_{r_0(k)}(e) \text{ and } \partial_n v_h|_e \in \mathbb{P}_{r_1(k)}(e) \quad \forall e \in \partial E \right\}, \quad (9)$$

for $k \geq 2$, where we let $r_0(k)$ and $r_1(k)$ be the two integer-valued functions of the integer k such that

$$r_0(k) = \begin{cases} 3 & \text{if } k = 2, \\ k & \text{if } k \geq 3, \end{cases} \quad r_1(k) = k - 1, \quad \text{if } k \geq 2.$$

The dimension of the local virtual element space $B_r^h(\partial E)$ is equal to

$$\dim B_k^h(\partial E) = N_E^{\mathcal{E}}(r_0(k) + r_1(k) + 2) - 3N_E^{\mathcal{V}} = N_E^{\mathcal{E}}(r_0(k) + r_1(k) - 1),$$

where $N_E^{\mathcal{E}}$ and $N_E^{\mathcal{V}}$ are the number of edges and vertices of the polygonal boundary ∂E (note that $N_E^{\mathcal{E}} = N_E^{\mathcal{V}}$). The term $-3N_E^{\mathcal{V}}$ takes into consideration the constraint $v_h \in C^1(\partial E)$.

Examples for different values of k are the following ones:

- for $k = 2$, we find that $r_0(2) = 3$, $r_1(2) = 1$, and

$$B_2^h(\partial E) := \left\{ v_h \in C^1(\partial E) \text{ such that } v_h|_e \in \mathbb{P}_3(e) \text{ and } \partial_n v_h|_e \in \mathbb{P}_1(e) \quad \forall e \in \partial E \right\};$$



Figure 1: Edge degrees of freedom **(D1)**-**(D2)** of the virtual element space $V_k^h(\mathbf{E})$ with polynomial degree k such that $2 \leq k \leq 5$. The (green) dots at the vertices represent the vertex values and each (red) vertex circle represents an order of derivation. The (black) dots on the edge represent the polynomial moments of the trace $v_{h|e}$; the arrows represent the polynomial moments of $\partial_n v_{h|e}$.

- for $k = 3$, we find that $r_0(3) = 3$, $r_1(3) = 2$, and

$$B_3^h(\partial\mathbf{E}) := \left\{ v_h \in C^1(\partial\mathbf{E}) \text{ such that } v_{h|e} \in \mathbb{P}_3(e) \text{ and } \partial_n v_{h|e} \in \mathbb{P}_2(e) \forall e \in \partial\mathbf{E} \right\};$$

- for $k = 4$, we find that $r_0(4) = 4$, $r_1(4) = 3$, and

$$B_4^h(\partial\mathbf{E}) := \left\{ v_h \in C^1(\partial\mathbf{E}) \text{ such that } v_{h|e} \in \mathbb{P}_4(e) \text{ and } \partial_n v_{h|e} \in \mathbb{P}_3(e) \forall e \in \partial\mathbf{E} \right\}.$$

Then, we consider the differential operator

$$\mathcal{L}(v) = (\alpha_2 \Delta^2 - \alpha_1 \Delta)v,$$

(where we recall that $\alpha_2, \alpha_1 > 0$). For all the integers $k \geq 2$, we consider

$$\tilde{V}_k^h(\mathbf{E}) := \left\{ v_h \in H^2(\mathbf{E}) : \mathcal{L}v_h \in \mathbb{P}_k(\mathbf{E}), v_{h|e} \in B_k^h(\partial\mathbf{E}) \right\}.$$

On every mesh element $\mathbf{E} \in \Omega_h$, we consider the set of real valued, linear and continuous functionals that associates a function $v \in H^2(\mathbf{E})$ with

(D1): for $k \geq 2$, $v(\mathbf{x}_v)$, $\partial_x v(\mathbf{x}_v)$, $\partial_y v(\mathbf{x}_v)$ for any vertex v of $\partial\mathbf{E}$;

(D2): for $k \geq 4$, $\frac{1}{h_e} \int_e qv ds$ for any $q \in \mathbb{P}_{k-4}(e)$, and any edge $e \in \partial\mathbf{E}$;

(D3): for $k \geq 3$, $\int_e q \partial_n v ds$ for any $q \in \mathbb{P}_{k-3}(e)$, and any edge $e \in \partial\mathbf{E}$;

(D4): for $k \geq 2$, $\frac{1}{|\mathbf{E}|} \int_{\mathbf{E}} qv d\mathbf{x}$ for any $q \in \mathbb{P}_{k-2}(\mathbf{E})$.

Figure 1 shows the degrees of freedom **(D1)**-**(D3)** associated with a given mesh edge e . We note that the traces $v_{h|e} \in \mathbb{P}_{r_0(k)}(e)$ and $\partial_n v_{h|e} \in \mathbb{P}_{r_1(k)}(e)$ are computable using the values of **(D1)**-**(D3)**. For all $v \in H^2(\mathbf{E})$, the L^2 -orthogonal projection $\Pi_{k-2}^0 v$ is computable using the values of **(D4)**.

Now, consider the integer $k \geq 2$ and the bilinear form $\mathcal{B}(u, v) = \alpha_2 \mathcal{A}_2(u, v) + \alpha_1 \mathcal{A}_1(u, v)$ with $\alpha_2, \alpha_1 > 0$. We define the elliptic projection operator $\Pi_k^{\mathcal{L}, \mathbf{E}} : H^2(\mathbf{E}) \rightarrow \mathbb{P}_k(\mathbf{E})$ such that for every $v \in H^2(\mathbf{E})$, the k -degree polynomial $\Pi_k^{\mathcal{L}, \mathbf{E}} v$ is the solution to the variational problem:

$$\mathcal{B}(\Pi_k^{\mathcal{L}, \mathbf{E}} v - v, q) = 0 \quad \forall q \in \mathbb{P}_k(\mathbf{E}), \quad (10)$$

$$\int_{\partial\mathbf{E}} (\Pi_k^{\mathcal{L}, \mathbf{E}} v - v) ds = 0. \quad (11)$$

Remark 3.1. Equation (10) defines the elliptic projection operator $\Pi_k^{\mathcal{L},E}(\cdot)$ up to constant functions on E since we assume that $\alpha_1 > 0$. This fact will be reflected by the way we fix the kernel of such projector in the practical implementation of the method, cf. Section 5; see also [3]. If we relax this condition and assume that only α_2 is strictly positive and α_1 is nonnegative, i.e., $\alpha_1 \geq 0$, then the solution to (10) is defined up to the harmonic polynomials $\mathbb{P}_k^H(E) = \{q \in \mathbb{P}_k(E) : \Delta q = 0\}$, which is a subspace of $\mathbb{P}_k(E)$. For example, for $\alpha_1 = 0$, $k = 2$ and $q = xy$, Equation (10) is satisfied independently of the definition of $\Pi_k^{\mathcal{L},E}v_h$ since $\Delta(xy) = 0$. In such a case, we should supplement (10)-(11) with a condition that removes the indeterminacy due to the harmonic polynomials or redefine (10) by taking q in the quotient space $\mathbb{P}_k(E) \setminus \mathbb{P}_k^H(E)$.

Remark 3.2. In this article, we have defined the projector $\Pi_k^{\mathcal{L},E}$ using the differential operator \mathcal{L} . To define the projector uniquely, we affix one additional equation, i.e., (11), to remove the kernel of \mathcal{L} . The technique employed here can be extended to approximate the operator $\mathcal{L} + \alpha_0 u$ whenever $\alpha_0 > 0$. In such a case, the projector $\Pi_k^{\mathcal{L},E}$ is defined uniquely by (10), and we do not need to fix any kernel. However, in this work we do not pursue this approach since we want to keep the possibility that $\alpha_0 = 0$.

The polynomial $\Pi_k^{\mathcal{L},E}v_h$ is computable for every $\tilde{v}_h \in \tilde{V}_k^h(E) \subset H^2(E)$ using the values of the functionals (D1)-(D4). In fact, let $q \in \mathbb{P}_k(E)$, $v_h \in \tilde{V}_k^h(E)$. A repeated integration by parts yields

$$\begin{aligned} \mathcal{B}(v_h, q) &= \int_E v_h (\alpha_2 \Delta^2 q - \alpha_1 \Delta q) \, d\mathbf{x} + \int_{\partial E} \left(v_h \partial_n (\alpha_1 q - \alpha_2 \Delta q) + \alpha_2 (\partial_n v_h) \Delta q \right) \, ds \\ &= \int_E v_h \mathcal{L}q \, d\mathbf{x} + \int_{\partial E} \left(v_h \partial_n (\alpha_1 q - \alpha_2 \Delta q) + \alpha_2 (\partial_n v_h) \Delta q \right) \, ds. \end{aligned}$$

On the one hand, the volume integral on the right is computable using the values of (D4) since $\mathcal{L}q \in \mathbb{P}_{k-2}(E)$. On the other hand, the boundary integral on the right is computable since the values of (D1)-(D3) for v_h allow us to compute the polynomial trace of v_h and $\partial_n v_h$ in $\mathbb{P}_{r_0(k)}(\mathbf{e})$ and $\mathbb{P}_{r_1(k)}(\mathbf{e})$, respectively, on every edge $\mathbf{e} \in \partial E$.

Now, let $\mathbb{P}_k(E) \setminus \mathbb{P}_{k-2}(E)$ denote the space of the polynomials of degree k that are orthogonal to the polynomials of degree $k-2$, and consider the linear functionals providing the values:

- (D4): for $k \geq 4$, $\frac{1}{|E|} \int_E qv \, d\mathbf{x}$ for any $q \in \mathbb{P}_k(E) \setminus \mathbb{P}_{k-2}(E)$.

For notation convenience, we introduce $(\widetilde{\mathbf{D4}}) = [(\mathbf{D4}), (\overline{\mathbf{D4}})]$ to collect all the functionals associated with the internal moments. Furthermore, we let $\widetilde{\mathcal{D}} = [(\mathbf{D1}), (\mathbf{D2}), (\mathbf{D3}), (\widetilde{\mathbf{D4}})]$ be the set of the values provided by all the functionals defined so far. The following lemma states that these functionals are unisolvent in $\tilde{V}_k^h(E)$, and can thus be taken as the degrees of freedom of this space.

Lemma 3.3 (Unisolvency of $\widetilde{\mathcal{D}}$ in $\tilde{V}_k^h(E)$). Each function $v_h \in \tilde{V}_k^h(E)$ is uniquely determined by the degrees of freedom $\widetilde{\mathcal{D}}$.

Proof. From a counting argument, we note that the cardinality of $\widetilde{\mathcal{D}}$ equals the dimension of $\tilde{V}_k^h(E)$. Then, take $v_h \in \tilde{V}_k^h(E)$, $k \geq 2$. A repeated integration by parts yields

$$\begin{aligned} \mathcal{B}(v_h, v_h) &= \int_E (\alpha_2 |\Delta v_h|^2 + \alpha_1 |\nabla v_h|^2) \, d\mathbf{x} = \int_E v_h (\alpha_2 \Delta^2 v_h - \alpha_1 \Delta v_h) \, d\mathbf{x} \\ &\quad + \int_{\partial E} \left(v_h \partial_n (\alpha_1 v_h - \alpha_2 \Delta v_h) + \alpha_2 (\partial_n v_h) \Delta v_h \right) \, ds. \end{aligned}$$

Let all the values provided by $\widetilde{\mathcal{D}}$ for v_h be equal to zero. All the polynomial moments of degree (up to) k of v_h are zero since the values $(\widetilde{\mathbf{D4}})$ for v_h are zero. The volume integral is zero because it is the moment of v_h against $\mathcal{L}v_h = \alpha_2 \Delta^2 v_h - \alpha_1 \Delta v_h$, which is a polynomial of degree k from the space definition. The boundary integrals are zero because assuming that $(\mathbf{D1})$ - $(\mathbf{D3})$ are equal to zero implies that all the edge traces of v_h and $\partial_n v_h$ are zero. Therefore, $\nabla v_h = 0$, so that v_h is constant on E . This constant must be zero since a constant function equals all its degrees of freedom (not implying a derivative) that we suppose to be zero. \square

3.2. Enhanced virtual element space

The enhanced virtual element space is

$$V_k^h(E) := \left\{ v_h \in \widetilde{V}_k^h(E) : \int_E (v_h - \Pi_k^{\mathcal{L},E} v_h) q \, d\mathbf{x} = 0 \quad \forall q \in \mathbb{P}_k(E) \setminus \mathbb{P}_{k-2}(E) \right\}. \quad (12)$$

A few noteworthy properties follow from this definition. The polynomial space $\mathbb{P}_k(E)$ is a subspace of $V_k^h(E)$. The H^2 -orthogonal projection operator $\Pi_k^{\mathcal{L},E} : \widetilde{V}_k^h(E) \rightarrow \mathbb{P}_k(E)$ is computable using only the degrees of freedom $(\mathbf{D1})$ - $(\mathbf{D4})$ and it is, thus, independent of the additional degrees of freedom $(\widetilde{\mathbf{D4}})$. The L^2 -orthogonal projection operator $\Pi_k^{0,E} : V_k^h(E) \rightarrow \mathbb{P}_k(E)$ is computable using only the degrees of freedom $(\mathbf{D1})$ - $(\mathbf{D4})$ and is also independent of the additional degrees of freedom $(\widetilde{\mathbf{D4}})$. Finally, as formally stated in the following lemma, the functionals providing the values of $(\mathbf{D1})$ - $(\mathbf{D4})$ are linearly independent on $V_k^h(E)$ and their number equals the dimension of $V_k^h(E)$. As a consequence, they are unisolvent in $V_k^h(E)$ and we can choose them as the degrees of freedom for this space.

Lemma 3.4. *The linear functionals providing the values of $(\mathbf{D1})$ - $(\mathbf{D4})$ are linearly independent in $V_k^h(E)$.*

Proof. Let $v_h \in V_k^h(E)$ such that all the values provided by the functionals $(\mathbf{D1})$ - $(\mathbf{D4})$ are zero. We only need to prove that $v_h = 0$. To this end, we first note that $\Pi_k^{\mathcal{L},E} v_h = 0$ as this polynomial projection only depends on the functionals returning the values of $(\mathbf{D1})$ - $(\mathbf{D4})$ (see the computability of $\Pi_k^{\mathcal{L},E}$). Since $\Pi_k^{\mathcal{L},E} v_h = 0$, the definition of $V_k^h(E)$ implies that

$$\int_E q v_h \, d\mathbf{x} = \int_E q \Pi_k^{\mathcal{L},E} v_h \, d\mathbf{x} = 0 \quad \forall q \in \mathbb{P}_k(E) \setminus \mathbb{P}_{k-2}(E). \quad (13)$$

Hence, the values of the functionals $(\widetilde{\mathbf{D4}})$ of v_h must also be equal to zero. Since all functionals $(\mathbf{D1})$, $(\mathbf{D2})$, $(\mathbf{D3})$, $(\widetilde{\mathbf{D4}})$ are zero for $v_h \in V_k^h(E) \subset \widetilde{V}_k^h(E)$, and these functionals are unisolvent in $\widetilde{V}_k^h(E)$, it follows that $v_h = 0$. \square

Let $\mathcal{D} = [(\mathbf{D1}), (\mathbf{D2}), (\mathbf{D3}), (\mathbf{D4})]$ denote the set of the linear functionals associated with the degrees of freedom for $V_k^h(E)$. In view of Lemma 3.4, we conclude that the triplet $(E, V_k^h(E), \mathcal{D})$ is a finite element in the sense of Ciarlet, cf. [23, Chapter 3].

The global virtual element space for $k \geq 2$ is given by

$$V_k^h := \left\{ v_h \in H^2(\Omega) : v_h|_E \in V_k^h(E) \quad \forall E \in \Omega_h \right\}. \quad (14)$$

The degrees of freedom of the functions in V_k^h are obtained by an H^2 -conforming coupling of the elemental degrees of freedom and are thus provided by the values of the functionals:

(D1): for $k \geq 2$, $v_h(\mathbf{x}_v)$, $\partial_x v_h(\mathbf{x}_v)$, $\partial_y v_h(\mathbf{x}_v)$ for any vertex v of \mathcal{V} ;

(D2): for $k \geq 4$, $\frac{1}{h_e} \int_e q v_h ds$ for any $q \in \mathbb{P}_{k-4}(e)$, and any edge $e \in \mathcal{E}$;

(D3): for $k \geq 3$, $\int_e q \partial_n v_h ds$ for any $q \in \mathbb{P}_{k-3}(e)$, and any edge $e \in \mathcal{E}$;

(D4): for $k \geq 2$, $\frac{1}{|E|} \int_E q v_h dx$ for any $q \in \mathbb{P}_{k-2}(E)$ and any $E \in \Omega_h$.

The sign of the normal derivative $\partial_n v_h$ along the edge e is determined by the global edge orientation and may differ by a factor -1 from its elementwise value. The unisolvence of (D1)-(D4) in V_k^h is an immediate consequence of their unisolvence at the elemental level. The unisolvence property implies the existence of a global Lagrangian basis $\varphi_1, \varphi_2, \dots, \varphi_{N^{\text{dofs}}}$ (in a global numbering system) where N^{dofs} is the total number of degrees of freedom, and such that the i -th basis function φ_i has all degrees of freedom equal to zero except the i -th one whose value is 1. The existence of such a set of basis functions, although virtual, is crucial in the implementation of the method.

3.3. Virtual element approximation of $\mathcal{A}(\cdot, \cdot)$ and $\mathcal{F}(\cdot)$

Let $E \in \Omega_h$ be a mesh element, and consider the bilinear forms $\mathcal{A}_2^E, \mathcal{A}_1^E, \mathcal{A}_0^E : V_k^h(E) \times V_k^h(E) \rightarrow \mathbb{R}$ given by integrating on E instead of Ω in the corresponding bilinear forms in (4). Let $\mathcal{A}^E(\cdot, \cdot) = \alpha_2 \mathcal{A}_2^E(\cdot, \cdot) + \alpha_1 \mathcal{A}_1^E(\cdot, \cdot) + \alpha_0 \mathcal{A}_0^E(\cdot, \cdot)$. We use the elliptic projection $\Pi_k^{\mathcal{L},E}$ and the L^2 -orthogonal projection $\Pi_k^{0,E}$ to define the virtual element bilinear form $\mathcal{A}_h^E : V_k^h(E) \times V_k^h(E) \rightarrow \mathbb{R}$:

$$\begin{aligned} \mathcal{A}_h^E(u_h, v_h) := & \alpha_2 \mathcal{A}_2^E(\Pi_k^{\mathcal{L},E} u_h, \Pi_k^{\mathcal{L},E} v_h) + \alpha_1 \mathcal{A}_1^E(\Pi_k^{\mathcal{L},E} u_h, \Pi_k^{\mathcal{L},E} v_h) + \alpha_0 \mathcal{A}_0^E(\Pi_k^{0,E} u_h, \Pi_k^{0,E} v_h) \\ & + S_h^E \left(u_h - \Pi_k^{\mathcal{L},E} u_h, v_h - \Pi_k^{\mathcal{L},E} v_h \right). \end{aligned}$$

Herein, the stabilization term is also built by using the projection $\Pi_k^{\mathcal{L},E}(v_h)$, and the usual formula, so that the bilinear form $S_h^E : V_k^h(E) \times V_k^h(E) \rightarrow \mathbb{R}$ can be any symmetric, positive definite, bilinear form such that

$$\sigma_* \mathcal{B}^E(v_h, v_h) \leq S_h^E(v_h, v_h) \leq \sigma^* \mathcal{B}^E(v_h, v_h) \quad \forall v_h \in V_k^h(E) \text{ with } \Pi_k^{\mathcal{L},E} v_h = 0, \quad (15)$$

where σ_* and σ^* are two positive constants independent of h (and the chosen E).

The bilinear form $\mathcal{A}_h^E(\cdot, \cdot)$ has the two major properties:

(i) **k -Consistency**: for every polynomial $q \in \mathbb{P}_k(E)$ and virtual element function $v_h \in V_k^h(E)$ it holds:

$$\mathcal{A}_h^E(v_h, q) = \mathcal{A}^E(v_h, q); \quad (16)$$

(ii) **Stability**: there exist two positive constants β_* , β^* independent of h (and E) such that for every $v_h \in V_k^h(E)$ it holds:

$$\beta_* \mathcal{A}^E(v_h, v_h) \leq \mathcal{A}_h^E(v_h, v_h) \leq \beta^* \mathcal{A}^E(v_h, v_h). \quad (17)$$

It is immediate to check that for example (17) holds by taking

$$\beta_* = \min(\alpha_0, \alpha_1, \alpha_2, \sigma_*) \quad \text{and} \quad \beta^* = \max(\alpha_0, \alpha_1, \alpha_2, \sigma^*).$$

A straightforward consequence of the stability condition (ii) stated above, is that the discrete bilinear form $\mathcal{A}_h^E(\cdot, \cdot)$ is continuous and coercive. These properties extend to the global virtual element bilinear form $\mathcal{A}_h : V_k^h \times V_k^h \rightarrow \mathbb{R}$ that we define by adding all the local terms,

$$\mathcal{A}_h(u_h, v_h) := \sum_{E \in \Omega_h} \mathcal{A}_h^E(u_h, v_h), \quad \forall u_h, v_h \in V_k^h.$$

We will find it useful to consider the local and global, discrete bilinear forms $\mathcal{B}_h^E : V_k^h(E) \times V_k^h(E) \rightarrow \mathbb{R}$, for all $E \in \Omega_h$, and $\mathcal{B}_h : V_k^h \times V_k^h \rightarrow \mathbb{R}$ that are such that

$$\mathcal{A}_h^E(u_h, v_h) = \mathcal{B}_h^E(u_h, v_h) + \alpha_0 \mathcal{A}_0^E(\Pi_k^{0,E} u_h, \Pi_k^{0,E} v_h), \quad (18)$$

$$\mathcal{A}_h(u_h, v_h) = \mathcal{B}_h(u_h, v_h) + \alpha_0 \mathcal{A}_0(\Pi_k^0 u_h, \Pi_k^0 v_h), \quad (19)$$

where $\Pi_k^{0,E} v_h$ is the L^2 -orthogonal projection of v_h onto the local polynomial subspace $\mathbb{P}_k(E)$ of $V_k^h(E)$; $\Pi_k^0 v_h$ is the global L^2 -orthogonal projection onto the space of k -degree piecewise polynomials $\mathbb{P}_k(\Omega_h)$ such that $(\Pi_k^0 v_h)|_E = \Pi_k^{0,E}(v_h|_E)$ for all $E \in \Omega_h$. Since $\mathcal{B}_h^E(\cdot, \cdot)$ and $\mathcal{B}_h(\cdot, \cdot)$ have the same stabilization term of $\mathcal{A}_h^E(\cdot, \cdot)$ and $\mathcal{A}_h(\cdot, \cdot)$, it is immediate to see that they satisfy the same consistency and stability properties (with slightly different constants) stated above as (i) and (ii), and clearly

$$\mathcal{B}_h(u_h, v_h) := \sum_{E \in \Omega_h} \mathcal{B}_h^E(u_h, v_h), \quad \forall u_h, v_h \in V_k^h.$$

The bilinear form $\mathcal{B}_h(\cdot, \cdot)$ is also globally continuous and coercive.

Assuming that $f \in H^{k-1}(\Omega)$, we approximate the right-hand side of (2) through the piecewise L^2 -orthogonal projection $f_h|_E = \Pi_{k-2}^{0,E} f$ for all $E \in \Omega_h$, so that

$$\langle f_h, v_h \rangle := \sum_{E \in \Omega_h} \langle f_h, v_h \rangle_E, \quad \langle f_h, v_h \rangle_E = \int_E f \Pi_{k-2}^{0,E} v_h \, dx. \quad (20)$$

3.4. Well-posedness

We conclude this section with the well-posedness result. The well-posedness of the discrete VEM (8) directly follows from the global coercivity and continuity of $\mathcal{A}_h(\cdot, \cdot)$ and the boundedness of $\langle f_h, \cdot \rangle$, as stated in the next proposition.

Proposition 3.5. *The VEM (8) with the previous definitions of $\mathcal{A}_h(\cdot, \cdot)$ and $\langle f_h, \cdot \rangle$ is well-posed.*

Proof. This result is a direct consequence of the Lax-Milgram Theorem, cf. [19, Theorem 2.7.7]. \square

4. Convergence analysis

In this section, we prove the convergence of the VEM by quantifying the error associated with the discrete scheme (8). Upon exploiting the coercivity and continuity of the discrete bilinear form $\mathcal{A}_h(\cdot, \cdot)$, we bound the term $|u - u_h|_{2,\Omega}$. Then, by using the duality argument, and the previous estimate of $|u - u_h|_{2,\Omega}$, we derive the error estimates in L^2 norm and H^1 seminorm assuming that the domain Ω is convex. To prove such estimates, we need the regularity results associated with the biharmonic problem

$$\begin{aligned} \alpha_2 \Delta^2 \xi - \alpha_1 \Delta \xi + \alpha_0 \xi &= g, & \text{in } \Omega, \\ \xi = \partial_n \xi &= 0, & \text{on } \Gamma. \end{aligned}$$

Since Ω is a convex domain, and according to the regularity results in [31], we know that

- the regularity result holds:

$$g \in H^{-1}(\Omega) \implies \xi \in H^3(\Omega) \quad \text{and} \quad \|\xi\|_{3,\Omega} \leq C\|g\|_{-1,\Omega}; \quad (21)$$

- there exists a real number s , with $0 < s \leq 1$, such that

$$g \in L^2(\Omega) \implies \xi \in H^{3+s}(\Omega) \quad \text{and} \quad \|\xi\|_{3+s,\Omega} \leq C\|g\|_{0,\Omega}. \quad (22)$$

The values of s depends on the maximum angle in Ω . If the maximum angle is strictly less than π , then $s = 1$ and $\xi \in H^4(\Omega)$.

4.1. Mesh assumptions

For the convergence analysis, we assume that the mesh family $\{\Omega_h\}_{0 < h \leq 1}$ satisfies the following regularity condition.

Assumption 4.1 (Mesh regularity). *There exists a positive real number ρ independent of h such that for every $E \in \Omega_h$, it holds that*

(A1) *star-shapedness:* E is star-shaped with respect to an internal ball with radius bigger than ρh_E ;

(A2) *uniform scaling:* the edge length h_e for all $e \in \partial E$ is bounded from below by ρh_E , i.e., $h_e \geq \rho h_E$.

A consequence of these properties is that the element E admits a uniformly shape-regular subtriangulation, i.e., the minimum angle of all the subtriangles partitioning E is bounded from below by some positive constant independent of h (and E).

4.2. A priori error estimates

The convergence of the virtual element method, which we state in Theorem 4.5 below, follows from the (standard) error bounds for the polynomial projection and interpolation operators stated in two technical lemmas, e.g., Lemma 4.2 and Lemma 4.3, which we report below for completeness without proof (for a proof, see [1, 20]) and the abstract convergence result of Lemma 4.4. To ease the notation, in both lemma statements we adopt the convention $|\cdot|_{0,E} = \|\cdot\|_{0,E}$ to denote the L^2 -norm over E .

Lemma 4.2 (Polynomial Approximation). *Under mesh regularity assumptions (A1)-(A2), see Assumption 4.1, there exists a positive constant C independent of h such that for all $v \in H^\delta(E)$, δ being a real number such that $0 \leq \delta \leq k+1$, there exists a polynomial approximation $v_\pi \in \mathbb{P}_k(E)$, such that*

$$|v - v_\pi|_{\ell,E} \leq Ch_E^{\delta-\ell} |v|_{\delta,E}, \quad \ell = 0, \dots, [\delta],$$

where $[\delta]$ denotes the largest integer equal to or smaller than δ . The constant C may depend on the mesh regularity parameter ρ .

Lemma 4.3 (Virtual element interpolation). *Under mesh regularity assumptions (A1)-(A2), see Assumption 4.1, there exists a positive constant C independent of h such that for all $v \in H^\delta(E)$, δ being a real number such that $2 \leq \delta \leq k+1$, there exists a virtual element approximation $v_I \in V_k^h(E)$ such that*

$$|v - v_I|_{\ell,E} \leq Ch_E^{\delta-\ell} |v|_{\delta,E}, \quad \ell = 0, 1, 2.$$

The constant C may depend on the mesh regularity parameter ρ .

Lemma 4.4 (Abstract result). *Let u be the solution of the variational problem (2) and u_h the solution of the virtual element method (8) under mesh regularity assumptions (A1)-(A2). Then, there exists a positive constant $C > 0$, such that the (piecewise discontinuous) polynomial approximation $u_\pi \in \mathbb{P}_k(\Omega_h)$ from Lemma 4.2, and the interpolation approximation $u_I \in V_k^h$ of u from Lemma 4.3 satisfy the inequality*

$$|u - u_h|_{2,\Omega} \leq C \left(|u - u_I|_{2,\Omega} + |u - u_\pi|_{2,\Omega} + \|f - f_h\|_{(V_k^h)'} \right), \quad (23)$$

where $\|\cdot\|_{(V_k^h)'}$ denotes the norm of $(V_k^h)'$, the dual space of V_k^h .

Proof. Let u_I be the interpolant of u that satisfies Lemma 4.3, and set $\delta_h := u_h - u_I \in V_k^h$. Adding and subtracting u_I and using the Cauchy-Schwarz inequality yield

$$|u - u_h|_{2,\Omega} \leq |u - u_I|_{2,\Omega} + |\delta_h|_{2,\Omega}.$$

Lemma 4.3 provides the upper bound for the first term on the right-hand side, i.e., $|u - u_I|_{2,\Omega}$. Furthermore, by using the coercivity of $\mathcal{A}_h(\cdot, \cdot)$ with coercivity constant $C_\alpha = \min(\alpha_0, \alpha_1, \alpha_2)$, the definition of δ_h , equations (2) and (8), and the polynomial consistency of $\mathcal{A}_h(\cdot, \cdot)$, we find that

$$\begin{aligned} C_\alpha |\delta_h|_{2,\Omega}^2 &\leq \mathcal{A}_h(\delta_h, \delta_h) = \mathcal{A}_h(u_h, \delta_h) - \mathcal{A}_h(u_I, \delta_h) \\ &= f_h(\delta_h) - \sum_{E \in \Omega_h} \mathcal{A}_h^E(u_I - u_\pi, \delta_h) - \sum_{E \in \Omega_h} \mathcal{A}_h^E(u_\pi, \delta_h) \\ &= f_h(\delta_h) - f(\delta_h) - \sum_{E \in \Omega_h} \mathcal{A}_h^E(u_I - u_\pi, \delta_h) + \sum_{E \in \Omega_h} \mathcal{A}_h^E(u - u_\pi, \delta_h). \end{aligned}$$

We conclude the proof of inequality (23) by employing the continuity of $\mathcal{A}_h^E(\cdot, \cdot)$ and $\mathcal{A}^E(\cdot, \cdot)$. \square

The following theorem states the convergence of the virtual element method and an error estimate for the approximation error measured using the seminorm $|\cdot|_{2,\Omega}$ (which is a norm on $H_0^2(\Omega)$).

Theorem 4.5 (Convergence in H^2 -seminorm). *Let u be the solution of the variational problem (2) with $f \in H^{k-1}(\Omega)$ and u_h the solution of the virtual element method (8) under mesh regularity assumptions (A1)-(A2). Then, there exists a positive constant $C > 0$ such that*

$$|u - u_h|_{2,\Omega} \leq Ch^{k-1} \left(|u|_{k+1,\Omega} + \|f\|_{k-1,\Omega} \right).$$

The constant C is independent of h , but depends on the α -coefficients associated with the model problem, the mesh regularity constant ρ , and the stability constants of the bilinear form $\mathcal{A}_h(\cdot, \cdot)$.

Proof. The assertion of the theorem is a straightforward consequence of the abstract convergence result stated in Lemma 4.4, the error bounds from Lemmas 4.2 and 4.3, and a standard estimate of the source error term $\|f - f_h\|_{(V_k^h)'}$ in the right-hand side of inequality (23) along with the regularity of f (cf. [10]). \square

Theorem 4.6 (Convergence in H^1 -seminorm). *Let u be the solution of the variational problem (2) with $f \in H^{k-1}(\Omega)$ and u_h the solution of the virtual element method (8) under mesh regularity assumptions (A1)-(A2). Then, there exists a positive constant $C > 0$, such that*

$$|u - u_h|_{1,\Omega} \leq Ch^k \left(|u|_{k+1,\Omega} + \|f\|_{k-1,\Omega} \right). \quad (24)$$

The constant C is independent of h , but depends on the α -coefficients associated with the model problem, the mesh regularity constant ρ , and the stability constants of the bilinear form $\mathcal{A}_h(\cdot, \cdot)$.

Proof. To prove the assertion of the theorem, we use the duality argument. Let ξ be the solution of the variational formulation of the auxiliary problem

$$\alpha_2 \Delta^2 \xi - \alpha_1 \Delta \xi + \alpha_0 \xi = -\Delta(u - u_h) \quad \text{in } \Omega, \quad (25a)$$

$$\xi = \partial_n \xi = 0 \quad \text{on } \Gamma. \quad (25b)$$

From suitable hypothesis on Ω , and a standard regularity argument, see [30] and (21)-(22), we know that

$$\|\xi\|_{3,\Omega} \leq C \|\Delta(u - u_h)\|_{-1} \leq C \|u - u_h\|_{1,\Omega} \leq C |u - u_h|_{1,\Omega}, \quad (26)$$

where the last step follows from the Poincare inequality, i.e., $\|u - u_h\|_{0,\Omega} \leq C |u - u_h|_{1,\Omega}$, which holds because $u - u_h \in H_0^2(\Omega)$. For ξ at least in $H^3(\Omega)$, the following interpolation estimate holds:

$$\|\xi - \xi_I\|_{0,\Omega} + h_E \|\xi - \xi_I\|_{1,\Omega} + h_E^2 \|\xi - \xi_I\|_{2,\Omega} \leq C h_E^3 |\xi|_{3,\Omega}. \quad (27)$$

Note that $|u - u_h|_{1,\Omega}^2 = -(\Delta(u - u_h), u - u_h)_{0,\Omega}$ since the traces of $(u - u_h)$ and $\partial_n(u - u_h)$ are zero on the boundary of Ω . We multiply both sides of (25a) by $u - u_h$, integrate over Ω and integrate by parts the Δ^2 and Δ terms. Then, we add and subtract the virtual element interpolant $\xi_I \in V_r^h$, cf. Lemma 4.3, and we obtain

$$\begin{aligned} |u - u_h|_{1,\Omega}^2 &= -(\Delta(u - u_h), u - u_h)_{0,\Omega} \\ &= (\alpha_2 \Delta^2 \xi - \alpha_1 \Delta \xi + \alpha_0 \xi, u - u_h) \\ &= \alpha_2 \mathcal{A}_2(u - u_h, \xi) + \alpha_1 \mathcal{A}_1(u - u_h, \xi) + \alpha_0 \mathcal{A}_0(u - u_h, \xi), \\ &= \mathcal{A}(u - u_h, \xi - \xi_I) + \mathcal{A}(u - u_h, \xi_I) \\ &= \mathcal{A}(u - u_h, \xi - \xi_I) + \left((f, \xi_I) - (f_h, \xi_I) \right) + \left(\mathcal{A}_h(u_h, \xi_I) - \mathcal{A}(u_h, \xi_I) \right) \\ &= (\mathbf{T1}) + (\mathbf{T2}) + (\mathbf{T3}). \end{aligned} \quad (28)$$

To complete the proof of inequality (24), we derive an upper bound for the three terms **(T1)**, **(T2)**, **(T3)** separately.

We bound the first term as follows below by using the continuity of the bilinear forms $\mathcal{A}_0(\cdot, \cdot)$, $\mathcal{A}_1(\cdot, \cdot)$, and $\mathcal{A}_2(\cdot, \cdot)$, and (27) and (26):

$$\begin{aligned} (\mathbf{T1}) &= \mathcal{A}(u - u_h, \xi - \xi_I) = \alpha_2 \mathcal{A}_2(u - u_h, \xi - \xi_I) + \alpha_1 \mathcal{A}_1(u - u_h, \xi - \xi_I) + \alpha_0 \mathcal{A}_0(u - u_h, \xi - \xi_I) \\ &\leq C(\alpha_2) |u - u_h|_{2,\Omega} \|\xi - \xi_I\|_{2,\Omega} + C(\alpha_1) |u - u_h|_{1,\Omega} \|\xi - \xi_I\|_{1,\Omega} + C(\alpha_0) \|u - u_h\|_{0,\Omega} \|\xi - \xi_I\|_{0,\Omega} \\ &\leq C(\alpha_2) h^k |u|_{k+1,\Omega} |u - u_h|_{1,\Omega} + C(\alpha_1) h^2 |u - u_h|_{1,\Omega}^2 + C(\alpha_0) h^3 |u - u_h|_{1,\Omega}^2. \end{aligned}$$

Since we assume that $f \in H^{k-1}(\Omega)$, we bound the second term by noting that for all $k \geq 2$, the quantity $(f - \Pi_{k-2}^{0,E} f)$ is L^2 -orthogonal to the constant functions, e.g., $\Pi_0^{0,E} \xi_I$. Therefore, using the Cauchy-Schwarz inequality, the approximation properties of the interpolation operator, the L^2 -orthogonal projection operator, and (27) and (26) yield:

$$\begin{aligned} (\mathbf{T2}) &\leq \sum_{E \in \Omega_h} \int_E (f - \Pi_{k-2}^{0,E} f) (\xi_I - \Pi_0^{0,E} \xi_I) \, dx \leq \|f - \Pi_{k-2}^0 f\|_{0,\Omega} \|\xi_I - \Pi_0^0 \xi_I\|_{0,\Omega} \\ &\leq C h^{k-1} |f|_{k-1,\Omega} \left(\|\xi_I - \xi\|_{0,\Omega} + \|\xi - \Pi_0^0 \xi\|_{0,\Omega} + \|\Pi_0^0 (\xi - \xi_I)\|_{0,\Omega} \right) \\ &\leq C h^k |f|_{k-1,\Omega} |u - u_h|_{1,\Omega}. \end{aligned} \quad (29)$$

Finally, we bound the term **(T3)** by using the (local) polynomial consistency, which allows us to rewrite the term $\mathcal{A}_h(\cdot, \cdot)$ as follows

$$\mathbf{(T3)} = \sum_{E \in \Omega_h} \left(\mathcal{A}_h^E(u_h - u_\pi, \xi_I - \xi_\pi) + \mathcal{A}^E(u_\pi - u_h, \xi_I - \xi_\pi) \right). \quad (30)$$

An application of the continuity property of $\mathcal{A}_h(\cdot, \cdot)$ and $\mathcal{A}(\cdot, \cdot)$, the approximation properties of Lemmas 4.2, and 4.3, and (27) yield

$$\begin{aligned} |(\mathbf{T3})| &\leq C(\beta^*) [\mathcal{A}(u_h - u_\pi, u_h - u_\pi)]^{1/2} [\mathcal{A}(\xi_I - \xi_\pi, \xi_I - \xi_\pi)]^{1/2} \\ &\leq C(\beta^*) \left[\alpha_2 |u_h - u_\pi|_{2,\Omega}^2 + \alpha_1 |u_h - u_\pi|_{1,\Omega}^2 + \alpha_0 |u_h - u_\pi|_{0,\Omega}^2 \right]^{1/2} \\ &\quad \times \left[\alpha_2 |\xi_I - \xi_\pi|_{2,\Omega}^2 + \alpha_1 |\xi_I - \xi_\pi|_{1,\Omega}^2 + \alpha_0 |\xi_I - \xi_\pi|_{0,\Omega}^2 \right]^{1/2} \\ &\leq C(\beta^*, \alpha_2, \alpha_1, \alpha_0) h^k |u|_{k+1,\Omega} \left[\alpha_2 + \alpha_1 h^2 + \alpha_0 h^3 \right]^{1/2} |u - u_h|_{1,\Omega}. \end{aligned}$$

Finally, we substitute the upper bounds of terms **(T1)**, **(T2)**, and **(T3)** into (28), and obtain the assertion of the lemma for $h \rightarrow 0$. \square

Now, we focus to derive the convergence analysis in the L^2 norm.

Theorem 4.7 (Convergence in L^2 -norm). *Let u be the solution of the variational problem (2) with $f \in H^{k-1}(\Omega)$ and u_h the solution of the virtual element method (8) under mesh regularity assumptions 4.1 (as in Theorem 4.5). Then, the following estimates holds*

$$\|u - u_h\|_{0,\Omega} \leq Ch^2 \left(|u|_{3,\Omega} + \|f\|_{1,\Omega} \right) \quad \text{for } k = 2 \quad (31a)$$

$$\|u - u_h\|_{0,\Omega} \leq Ch^{k+s} \left(|u|_{k+1,\Omega} + \|f\|_{k-1,\Omega} \right) \quad \text{for } k \geq 3, \quad (31b)$$

where s is the regularity index of the function u as mentioned in (22).

Proof. Estimate (31a) directly follows from an application of Theorem 4.6, Eq. (24), and the Poincaré inequality $\|u - u_h\|_{0,\Omega} \leq C|u - u_h|_{1,\Omega}$, which holds since $u - u_h \in H_0^2(\Omega)$. To prove inequality (31b), we use the duality argument. Let $\xi \in H_0^2(\Omega)$ be the solution of the variational formulation of the auxiliary problem

$$\alpha_2 \Delta^2 \xi - \alpha_1 \Delta \xi + \alpha_0 \xi = -\Delta(u - u_h) \quad \text{in } \Omega, \quad (32a)$$

$$\xi = \partial_n \xi = 0 \quad \text{on } \Gamma. \quad (32b)$$

According to [22, 31], we deduce the following regularity result:

$$\|\xi\|_{3+s} \leq C \|u - u_h\|_{0,\Omega} \quad (33)$$

for some real number $s \in (1/2, 1]$. We multiply (32a) by $u - u_h$ and integrate over the domain Ω , and we find that

$$\|u - u_h\|_{0,\Omega}^2 = (u - u_h, u - u_h) = \left(\alpha_2 \Delta^2 \xi - \alpha_1 \Delta \xi + \alpha_0 \xi, u - u_h \right).$$

Using the same arguments of the derivation of (28), we obtain

$$\begin{aligned} \|u - u_h\|_{0,\Omega}^2 &= \mathcal{A}(u - u_h, \xi - \xi_I) + \left((f, \xi_I) - (f_h, \xi_I) \right) + \left(\mathcal{A}_h(u_h, \xi_I) - \mathcal{A}(u_h, \xi_I) \right) \\ &= \mathbf{(T1)} + \mathbf{(T2)} + \mathbf{(T3)}. \end{aligned} \quad (34)$$

Upon splitting the bilinear form $\mathcal{A}(\cdot, \cdot)$ into the H^2 -, H^1 -, and L^2 -scalar products, using the continuity of the bilinear forms, and again the interpolation estimate for $\xi - \xi_I$ and (33), we obtain that

$$\begin{aligned}
(\mathbf{T1}) &= \alpha_2 \mathcal{A}_2(u - u_h, \xi - \xi_I) + \alpha_1 \mathcal{A}_1(u - u_h, \xi - \xi_I) + \alpha_0 \mathcal{A}_0(u - u_h, \xi - \xi_I) \\
&\leq C(\alpha_2) h^{k+s} |u|_{k+1, \Omega} \|u - u_h\|_{0, \Omega} + C(\alpha_1) h^{k+s+1} |u|_{k+1, \Omega} \|u - u_h\|_{0, \Omega} \\
&\quad + C(\alpha_0) h^{k+s+2} \|u\|_{k+1, \Omega} \|u - u_h\|_{0, \Omega} \\
&\leq h^{k+s} \left(C(\alpha_2) |u|_{k+1, \Omega} + C(\alpha_1) h |u|_{k+1, \Omega} + C(\alpha_0) h^2 |u|_{k+1, \Omega} \right) \|u - u_h\|_{0, \Omega}. \quad (35)
\end{aligned}$$

Since we assume that $f \in H^{k-1}(\Omega)$, we bound the second term by noting that for all $k \geq 3$, the quantity $(f - \Pi_{k-2}^{0, E} f)$ is L^2 -orthogonal to the linear polynomial functions, e.g., $\Pi_1^{0, E} \xi_I$. Therefore, using the Cauchy-Schwarz inequality, the approximation properties of the interpolation operator, the L^2 -orthogonal projection operator, and (27) and (26) yield:

$$\begin{aligned}
(\mathbf{T2}) &\leq \sum_{E \in \Omega_h} \int_E (f - \Pi_{k-2}^{0, E} f) (\xi_I - \Pi_1^{0, E} \xi_I) dx \leq \|f - \Pi_{k-2}^0 f\|_{0, \Omega} \|\xi_I - \Pi_1^0 \xi_I\|_{0, \Omega} \\
&\leq Ch^{k-1} |f|_{k-1, \Omega} \left(\|\xi_I - \xi\|_{0, \Omega} + \|\xi - \Pi_1^0 \xi\|_{0, \Omega} + \|\Pi_1^0 (\xi - \xi_I)\|_{0, \Omega} \right) \\
&\leq Ch^k |f|_{k-1, \Omega} \|u - u_h\|_{0, \Omega}. \quad (36)
\end{aligned}$$

Finally, we proceed to estimate last term $(\mathbf{T3})$. To this end, we employ the polynomial consistency property of the discrete bilinear forms, the polynomial approximation property of Lemma 4.2, and the approximation property of the interpolation operator of Lemma 4.3, and we deduce

$$\begin{aligned}
(\mathbf{T3}) &\leq C(\beta^*) \left[\alpha_2 |u_h - u_\pi|_{2, \Omega}^2 + \alpha_1 |u_h - u_\pi|_{1, \Omega}^2 + \alpha_0 |u_h - u_\pi|_{0, \Omega}^2 \right]^{1/2} \\
&\quad \times \left[\alpha_2 |\xi_I - \xi_\pi|_{2, \Omega}^2 + \alpha_1 |\xi_I - \xi_\pi|_{1, \Omega}^2 + \alpha_0 |\xi_I - \xi_\pi|_{0, \Omega}^2 \right]^{1/2} \\
&\leq C(\beta^*) \left[\alpha_2 |u_h - u_\pi|_{2, \Omega}^2 + \alpha_1 |u_h - u_\pi|_{1, \Omega}^2 + \alpha_0 |u_h - u_\pi|_{0, \Omega}^2 \right]^{1/2} \\
&\quad \times h^{1+s} \left[\alpha_2 + \alpha_1 h^2 + \alpha_0 h^4 \right]^{1/2} \|\xi\|_{3+s, \Omega} \\
&\leq C(\beta^*, \alpha_2, \alpha_1, \alpha_0) h^{k+s} |u|_{k+1, \Omega} \|u - u_h\|_{0, \Omega}. \quad (37)
\end{aligned}$$

Upon inserting the estimates of (35), (36), and (37) into (34), we obtain the required result for $h \rightarrow 0$. \square

5. Implementation

In this section, we briefly describe how we implemented the VEM. The approach follows the general guidelines of [11], here adapted to the biharmonic problem.

5.1. Vector and matrix notation

We consider the following compact notation. For all element $E \in \Omega_h$, we locally number the degrees of freedom $(\mathbf{D1})$, $(\mathbf{D2})$, $(\mathbf{D3})$, and $(\mathbf{D4})$ from 1 to N^{dofs} . Then, we introduce the bounded, linear functionals $\text{dof}_i : V_k^h(E) \rightarrow \mathbb{R}$, $i = 1, \dots, N^{\text{dofs}}$, such that

$$\text{dof}_i(v_h) := i\text{-th degree of freedom of } v_h$$

for $v_h \in V_k^h(\mathbf{E})$. Let $\Lambda_{\mathbf{E}} = \{\text{dof}_i(\cdot)\}_i$ denote the set of such functionals and collect the degrees of freedom of v_h in the vector $\mathbf{v}_h = (\text{dof}_1(v_h), \dots, \text{dof}_{N^{\text{dofs}}}(v_h))^T$. Since the degrees of freedom **(D1)**, **(D2)**, **(D3)**, and **(D4)** are unisolvent in $V_k^h(\mathbf{E})$, the triplet $(\mathbf{E}, V_k^h(\mathbf{E}), \Lambda_{\mathbf{E}})$ is a finite element in the sense of Ciarlet, cf. [23]. This property implies the existence of a Lagrangian basis set $\{\varphi_i\}_i$, with $\varphi_i \in V_k^h(\mathbf{E})$, $i = 1, \dots, N^{\text{dofs}}$, which satisfies

$$\text{dof}_i(\varphi_j) = \delta_{ij}, \quad i, j = 1, 2, \dots, N^{\text{dofs}}.$$

We refer to the basis function set $\{\varphi_i\}_i$ as the ‘‘canonical’’ basis of $V_k^h(\mathbf{E})$. We introduce the compact notation

$$\boldsymbol{\varphi}(\mathbf{x}) = (\varphi_1(\mathbf{x}), \dots, \varphi_{N^{\text{dofs}}}(\mathbf{x}))^T,$$

and write the expansion of a virtual element function v_h on such a basis set as

$$v_h(\mathbf{x}) = \boldsymbol{\varphi}(\mathbf{x})^T \mathbf{v}_h = \sum_{i=1}^{N^{\text{dofs}}} \text{dof}_i(v_h) \varphi_i(\mathbf{x}) \quad \forall \mathbf{x} \in \mathbf{E}.$$

We also introduce a compact notation for the basis of the polynomial subspace $\mathbb{P}_k(\mathbf{E}) \subset V_k^h(\mathbf{E})$, which reads as

$$\mathbf{m}(\mathbf{x}) = (m_1(\mathbf{x}), \dots, m_{n_k}(\mathbf{x}))^T,$$

where n_k is the cardinality of $\mathbb{P}_k(\mathbf{E})$. Since the polynomials $m_\alpha(\mathbf{x})$ are also virtual element functions, we can expand them on the canonical basis $\boldsymbol{\varphi}$. We express such expansions as

$$\mathbf{m}(\mathbf{x})^T = \boldsymbol{\varphi}(\mathbf{x})^T \mathbf{D},$$

where matrix \mathbf{D} has size $N^{\text{dofs}} \times n_k$ and collects all the expansion coefficients

$$D_{i\ell} = \text{dof}_i(m_\ell),$$

so that

$$m_\ell(\mathbf{x}) = \sum_{i=1}^{N^{\text{dofs}}} \varphi_i(\mathbf{x}) D_{i\ell} \quad \ell = 1, \dots, n_k.$$

Following this notation, we also express the action of a differential operator \mathcal{D} , e.g., $\mathcal{D} = \Delta$ or $\mathcal{D} = \nabla$, in a entry-wise way, so that

$$\mathcal{D}\boldsymbol{\varphi}(\mathbf{x}) = (\mathcal{D}\varphi_1(\mathbf{x}), \dots, \mathcal{D}\varphi_{N^{\text{dofs}}}(\mathbf{x}))^T,$$

and

$$\mathcal{D}\mathbf{m}(\mathbf{x}) = (\mathcal{D}m_1(\mathbf{x}), \dots, \mathcal{D}m_{n_k}(\mathbf{x}))^T.$$

Similarly, we express the action of the projectors $\Pi_k^{\mathcal{L},\mathbf{E}}$, $\Pi_k^{\nabla,\mathbf{E}}$, and $\Pi_k^{0,\mathbf{E}}$ on the canonical basis functions $\boldsymbol{\varphi}$ and their expansion on the polynomial basis \mathbf{m} as follows:

$$\Pi_k^{\mathcal{L},\mathbf{E}} \boldsymbol{\varphi}^T = \left[\Pi_k^{\mathcal{L},\mathbf{E}} \varphi_1, \Pi_k^{\mathcal{L},\mathbf{E}} \varphi_2, \dots, \Pi_k^{\mathcal{L},\mathbf{E}} \varphi_{N^{\text{dofs}}} \right] = \mathbf{m}^T \mathbf{\Pi}_k^{\mathcal{L},\mathbf{E}},$$

$$\Pi_k^{\nabla,\mathbf{E}} \boldsymbol{\varphi}^T = \left[\Pi_k^{\nabla,\mathbf{E}} \varphi_1, \Pi_k^{\nabla,\mathbf{E}} \varphi_2, \dots, \Pi_k^{\nabla,\mathbf{E}} \varphi_{N^{\text{dofs}}} \right] = \mathbf{m}^T \mathbf{\Pi}_k^{\nabla,\mathbf{E}},$$

$$\Pi_k^{0,\mathbf{E}} \boldsymbol{\varphi}^T = \left[\Pi_k^{0,\mathbf{E}} \varphi_1, \Pi_k^{0,\mathbf{E}} \varphi_2, \dots, \Pi_k^{0,\mathbf{E}} \varphi_{N^{\text{dofs}}} \right] = \mathbf{m}^T \mathbf{\Pi}_k^{0,\mathbf{E}}.$$

The expansion coefficients for the three projection operators applied to the basis function φ_j are collected along the j -th column of the projection matrices $\mathbf{\Pi}_k^{\mathcal{L},\mathbf{E}}$, $\mathbf{\Pi}_k^{\nabla,\mathbf{E}}$, $\mathbf{\Pi}_k^{0,\mathbf{E}}$.

5.2. Elliptic projector operator

Using this compact notation, we rewrite the variational problem (10)-(11) that defines the polynomial projection $\Pi_k^{\mathcal{L},E}$ on the virtual element space $V_k^h(E)$ as $\mathbf{G}\Pi_k^{\mathcal{L},E} = \mathbf{B}$, where $\mathbf{G} = \tilde{\mathbf{G}} + \mathbf{G}^0 \in \mathbb{R}^{n_k \times n_k}$, $\mathbf{B} = \tilde{\mathbf{B}} + \mathbf{B}^0 \in \mathbb{R}^{n_k \times N^{\text{dofs}}}$, with

$$\tilde{\mathbf{G}} = \alpha_2 \tilde{\mathbf{G}}_2 + \alpha_1 \tilde{\mathbf{G}}_1 = \alpha_2 \int_E \Delta \mathbf{m} \Delta \mathbf{m}^T dx + \alpha_1 \int_E \nabla \mathbf{m} \cdot \nabla \mathbf{m}^T dx,$$

$$\tilde{\mathbf{B}} = \alpha_2 \tilde{\mathbf{B}}_2 + \alpha_1 \tilde{\mathbf{B}}_1 = \alpha_2 \int_E \Delta \mathbf{m} \Delta \varphi^T dx + \alpha_1 \int_E \nabla \mathbf{m} \cdot \nabla \varphi^T dx,$$

and

$$\mathbf{G}^0 = \begin{pmatrix} \widehat{\Pi_k^{\nabla,E} \mathbf{m}^T} \\ \mathbf{0}^T \\ \vdots \\ \mathbf{0}^T \end{pmatrix}, \quad \mathbf{B}^0 = \begin{pmatrix} \widehat{\Pi_k^{\nabla,E} \varphi^T} \\ \mathbf{0}^T \\ \vdots \\ \mathbf{0}^T \end{pmatrix},$$

We can split the linear system providing the projection matrix $\Pi_k^{\mathcal{L},E}$ into the summation of the two conditions $\tilde{\mathbf{G}}\Pi_k^{\mathcal{L},E} = \tilde{\mathbf{B}}$, which expresses (10), and $\mathbf{G}^0\Pi_k^{\mathcal{L},E} = \mathbf{B}^0$, which expresses (11). The latter condition fixes the kernel of the differential operator \mathcal{L} . Therefore, matrix \mathbf{G} is nonsingular by construction, and we can formally state that $\Pi_k^{\mathcal{L},E} = \mathbf{G}^{-1}\mathbf{B}$. A (double) integration by parts of the right-hand-side of the definition of $\tilde{\mathbf{B}}$ yields

$$\begin{aligned} \alpha_2 \tilde{\mathbf{B}}_2 + \alpha_1 \tilde{\mathbf{B}}_1 &= \alpha_2 \int_E \Delta \mathbf{m} \Delta \varphi^T dx + \alpha_1 \int_E \nabla \mathbf{m} \cdot \nabla \varphi^T dx \\ &= \int_E \left[\alpha_2 \Delta^2 \mathbf{m} - \alpha_1 \Delta \mathbf{m} \right] \varphi dx + \int_{\partial E} \left[(\partial_n(-\alpha_2 \mathbf{m} + \alpha_1 \mathbf{m})) \varphi^T + \alpha_2 \Delta \mathbf{m} (\partial_n \varphi^T) \right] dx. \end{aligned}$$

According to what has already been observed about the computability of the bilinear form $\mathcal{B}(v_h, q)$, we see that the last right-hand side above can be easily computable by an evaluation of the volume and surface integrals through the degrees of freedom of φ . We perform the numerical integration of the volume integral through the degrees of freedom (D4) and the numerical integration of the edge integrals by evaluating the trace of each basis function ϕ_i and its normal derivative $\partial_n \phi_i$ through the univariate polynomial interpolation of the degrees of freedom (D1), (D2), and (D3).

5.3. L^2 -orthogonal projector operator

Using this compact notation, we rewrite the variational problem (10)-(11) that defines the L^2 -orthogonal polynomial projection $\Pi_k^{0,E}$ on the virtual element space $V_k^h(E)$ as $\mathbf{H}\Pi_k^{0,E} = \mathbf{C}$, where

$$\mathbf{H} = \int_E \mathbf{m} \mathbf{m}^T dx \quad \text{and} \quad \mathbf{C} = \int_E \mathbf{m} \varphi^T dx.$$

We recall that the entries of matrix \mathbf{C} that correspond to the polynomial moments of the Lagrangian basis function φ against the polynomial of degree up to $k-2$ are computable from the degrees of freedom (D4). The enhancing condition in the definition of the local virtual element space (12) makes it possible to compute the polynomial moments of the basis functions φ against the polynomials of $\mathbb{P}_k(E) \setminus \mathbb{P}_{k-2}(E)$ by using the elliptic projector. Since matrix \mathbf{H} is nonsingular by construction, we can formally state that $\Pi_k^{0,E} = \mathbf{H}^{-1}\mathbf{C}$.

5.4. Local matrices

The stiffness matrix is given by the sum of two terms: a rank-deficient term, which is responsible for the accuracy of the method, and a stability term, which fixes the correct rank:

$$\mathbf{K}_E := \mathbf{K}_E^{\text{cons}} + \mathbf{K}_E^{\text{stab}},$$

where

$$(\mathbf{K}_E^{\text{cons}})_{ij} = \mathcal{B}_h^E(\Pi_k^{\mathcal{L},E} \varphi_i, \Pi_k^{\mathcal{L},E} \varphi_j) = \left((\mathbf{\Pi}_k^{\mathcal{L},E})^T \left[\alpha_2 \int_E \Delta \mathbf{m} \Delta \mathbf{m}^T d\mathbf{x} + \alpha_1 \int_E \nabla \mathbf{m} \cdot \nabla \mathbf{m}^T d\mathbf{x} \right] \mathbf{\Pi}_k^{\mathcal{L},E} \right)_{ij}$$

and

$$\begin{aligned} (\mathbf{K}_E^{\text{stab}})_{ij} &= S_h^E \left((I - \Pi_k^{\mathcal{L},E}) \varphi_i, (I - \Pi_k^{\mathcal{L},E}) \varphi_j \right) = \sum_{\ell} \text{dof}_{\ell} \left((I - \Pi_k^{\mathcal{L},E}) \varphi_i \right) \text{dof}_{\ell} \left((I - \Pi_k^{\mathcal{L},E}) \varphi_j \right) \\ &= \left((I - \mathbf{D}\mathbf{\Pi}_k^{\mathcal{L},E})^T (I - \mathbf{D}\mathbf{\Pi}_k^{\mathcal{L},E}) \right)_{ij}. \end{aligned}$$

The construction of the local mass matrix uses the L^2 -orthogonal projection:

$$(\mathbf{M}_E)_{ij} := (\mathbf{M}_E^{\text{cons}})_{ij} = \alpha_0 \mathcal{A}_0^E(\Pi_k^{0,E} \varphi_i, \Pi_k^{0,E} \varphi_j) = \left((\mathbf{\Pi}_k^{0,E})^T \left[\alpha_0 \int_E \mathbf{m} \mathbf{m}^T d\mathbf{x} \right] \mathbf{\Pi}_k^{0,E} \right)_{ij}.$$

Note that we do not need to specify a stabilization term in the local mass matrix.

5.5. Right-hand side approximation

Using again the compact notation, we rewrite the virtual element approximation of the right-hand side (20) as

$$\langle f_h, \varphi_i \rangle_E = \int_E f \Pi_k^{0,E} \varphi_i d\mathbf{x} = \left(\left[\int_E f \mathbf{m}^T d\mathbf{x} \right] \mathbf{\Pi}_k^{0,E} \right)_i. \quad (38)$$

5.6. Formulation of VEM in matrix representation

We assemble the local matrices \mathbf{K}_E and \mathbf{M}_E , the forcing term $\mathbf{F}_E = \langle f_h, \boldsymbol{\varphi} \rangle_E$ and incorporate the boundary conditions into the global matrices \mathbf{K} and \mathbf{M} and the right-hand side vector \mathbf{F} in a finite element way. The final linear system reads as:

$$(\mathbf{K} + \mathbf{M}) \mathbf{u}_h = \mathbf{F},$$

where \mathbf{u}_h is the vector collecting the degrees of freedom of the virtual element solution u_h . The final matrix $\mathbf{K} + \mathbf{M}$ is nonsingular by construction because of the stability property imposed on the local matrices $\mathbf{K}_E + \mathbf{M}_E$ and the boundary conditions.

6. Numerical Results

We investigate the behavior of the virtual element method on two manufactured test cases by numerically solving problem (2) with the virtual element method (8) described in Section 3. In the first test case, see Section 6.1, we study the convergence behavior of the method. In the second test case, see Section 6.2, we study the length-scale sensitivity of a bell-shaped crack-like solution.

In the first test case, we consider four representative mesh families including (a) smoothly remapped quadrilateral meshes; (b) randomized quadrilateral meshes; (c) smoothly remapped hexagonal meshes;

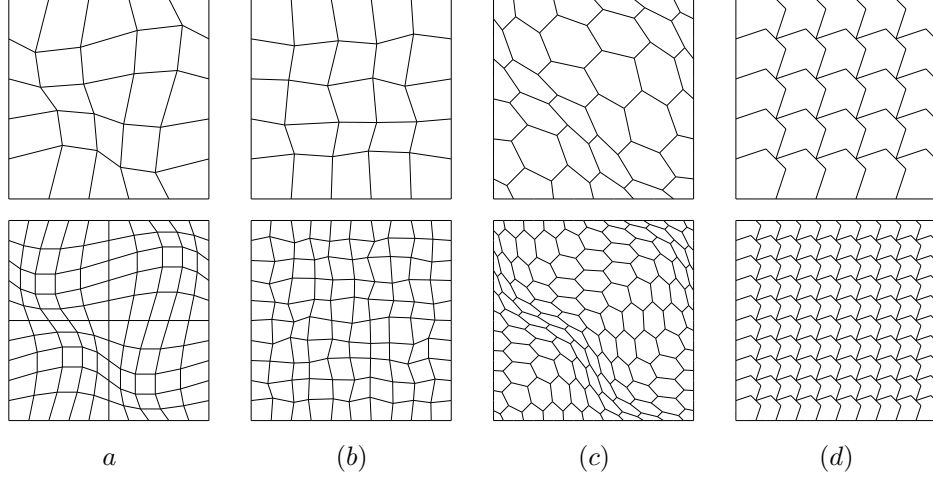


Figure 2: Base mesh (top panel) and first refinement (bottom panel) of (a) smoothly remapped quadrilateral mesh family; (b) randomized quadrilateral mesh family; (c) remapped hexagonal mesh family; (d) nonconvex octagonal mesh family.

(d) nonconvex octagonal meshes. In the second test case, we consider only the mesh families (b) and (c). The construction of these meshes and the way they are refined is rather standard, and details can easily be found in the virtual element literature, cf. [15]. For every mesh family, we consider a base mesh and eight refinements. Tables A.1, A.2, A.3, and A.4 in the final appendix report the mesh data and the number of degrees of freedom of the virtual element approximations with polynomial order $k = 2, 3, 4$. Figure 2 shows the base mesh (top panel) and the first refined mesh (bottom panel) of each mesh family.

On any set of refined meshes, we measure the relative errors in the L^2 , H^1 , and energy norms. Instead of the virtual element solution u_h , which is unknown, we use its orthogonal polynomial projection $\Pi_k^0 u_h$. We compute the L^2 relative error according to the formula

$$\text{error}_{L^2(\Omega)}(u_h) = \frac{\|u - \Pi_k^0 u_h\|_{0,\Omega}}{\|u\|_{0,\Omega}} \approx \frac{\|u - u_h\|_{0,\Omega}}{\|u\|_{0,\Omega}}; \quad (39)$$

the H^1 relative errors according to the formula

$$\text{error}_{H^1(\Omega)}(u_h) = \frac{|u - \Pi_k^0 u_h|_{1,h}}{|u|_{1,\Omega}} \approx \frac{|u - u_h|_{1,\Omega}}{|u|_{1,\Omega}}, \quad (40)$$

and the energy error according the formula

$$\text{error}_{\mathcal{A}_h}(u_h) = \left(\frac{\mathcal{A}_h(u - \Pi_k^0 u_h, u - \Pi_k^0 u_h)}{\mathcal{A}_h(u, u)} \right)^{\frac{1}{2}} \approx \frac{\|u - u_h\|_{2,\Omega}}{\|u\|_{2,\Omega}}. \quad (41)$$

6.1. Test Case 1. Convergence behavior of a manufactured solution in various norms

The nonhomogeneous Dirichlet boundary conditions and the source term are set on the computational domain $\bar{\Omega} = [0, 1] \times [0, 1]$ in accordance with the exact solutions

$$u(x, y) = \sin(2\pi x) \sin(2\pi y) + x^5 + y^5.$$

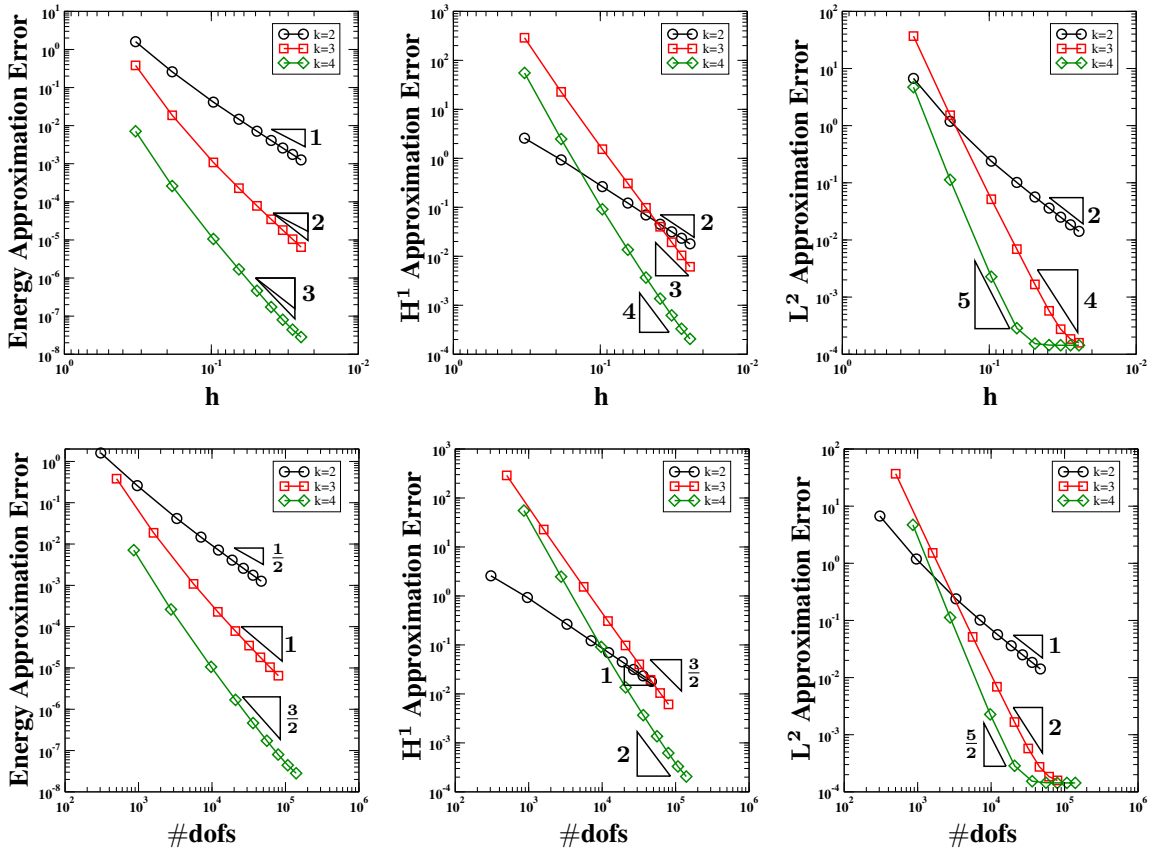


Figure 3: Test Case 1. Error curve measured using energy norm, H^2 norm, H^1 norm and L^2 norm. The calculations are carried out on the family of smoothly remapped quadrilateral meshes.

We apply the VEM on the four mesh families introduced in the previous section.

We show the log-log plots of the error curves for the four mesh families in Figures 3, 4, 5, and 6. In every figure, the three panels on top show the error curves versus the mesh size parameter h ; the three panels on bottom show the error curves versus the number of degrees of freedom, which is denoted by $\#\mathbf{dofs}$ on the axis of the plots. The slopes of these curves reflects the numerical convergence rate, while the triangles shown near such curves show the theoretical convergence rate according to the results of Theorems 4.7, 4.6, and 4.5. We recall that the convergence rate with respect to $\#\mathbf{dofs}$ is equal to the convergence rate with respect to h divided by two since we roughly have that $\#\mathbf{dofs} \simeq h^{-2}$. On some of the coarser meshes, the L^2 -norm errors for $k = 2$ are smaller than those produced by the VEM with $k = 3, 4$. This phenomenon probably occurs because the numerical method is working in a pre-asymptotic region. However, these numerical results are in good agreement with the theoretical predictions, and they show that the VEM proposed in this work provides the expected optimal convergence rate in the energy norm and lower-order norms on all the mesh families considered in this benchmark test. Since we can assume that the cost of solving the numerical method is somehow proportional to the number of degrees of freedom $\#\mathbf{dofs}$, the bottom plots show that on the finer meshes, the higher-order schemes are more convenient to achieve a pre-fixed accuracy level. We also note a *locking effect* in the convergence rate for $k = 4$ when we measure the error using the L^2 -norm. This effect is visible in all the meshes considered in our numerical experiments. This loss of convergence when the mesh is highly refined is very likely

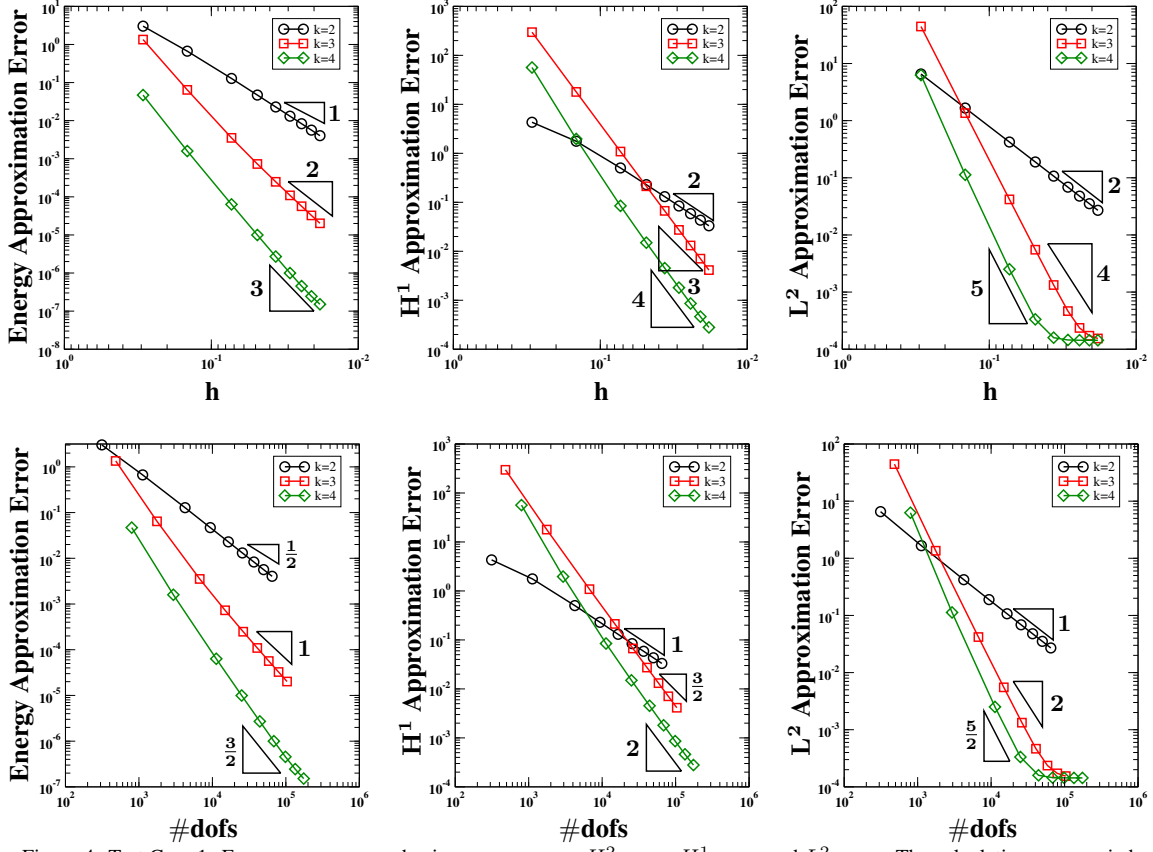


Figure 4: Test Case 1. Error curve measured using energy norm, H^2 norm, H^1 norm and L^2 norm. The calculations are carried out on the family of randomized quadrilateral meshes.

related to the increasing ill-conditioning of the linear system that we need to solve and will be the subject of further investigation.

6.2. Test Case 2. Diagonal crack example: Length-scale sensitivity

To showcase the merits of the VEM in PF fracture problems, a manufactured solution to HOPF equation is assumed as follows

$$u(x, y) = \exp(-(x - y)^2/\epsilon), \quad \epsilon \in \{1, 10^{-1}, 10^{-2}\}.$$

As illustrated in Figure 7(a), this function can be conceived as a PF approximation of a diagonal crack defined by the bisecting line $y = x$ and drawn in red color in the computational domain $\Omega = (0, 1) \times (0, 1)$. The length-scale parameter ϵ controls the width of the PF diffuse crack representation and can be decreased to approximate the sharp-crack limit. Figure 7(b) shows the solution u along line segment AB for $\epsilon = 10^{-2}$, where A and B are points depicted in 7(a). The non-homogeneous Dirichlet boundary conditions and source term shown in equation (1) are set in accordance with this exact solution.

In Figure 8, the proposed VEM is applied to the aforementioned problem on randomized quadrilateral meshes (2(b)) for different values of $\epsilon \in \{1, 10^{-1}, 10^{-2}\}$. The convergence curves are shown for the polynomial orders $k = 2, 3, 4$, from left to right, respectively. Similar numerical behavior is observed in Figure 9 for the VEM solution on smoothly remapped hexagonal meshes (2(c)).

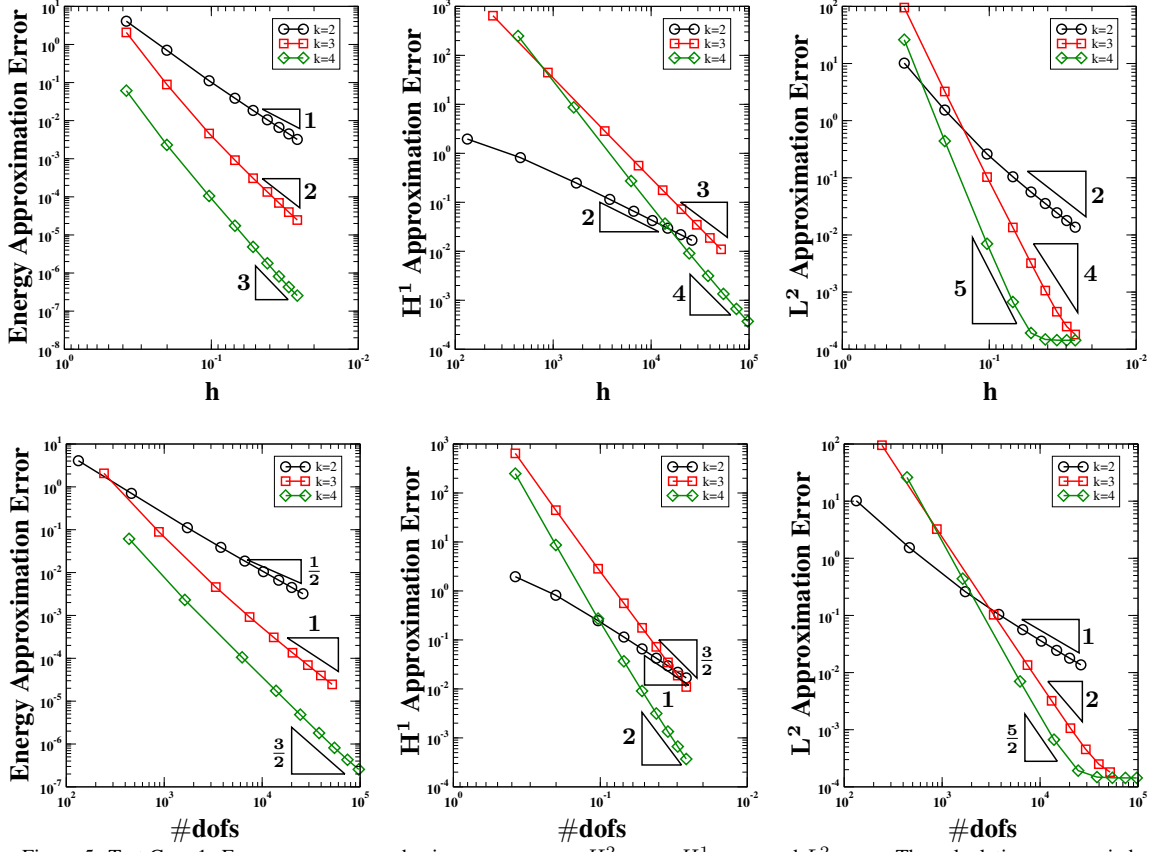


Figure 5: Test Case 1. Error curve measured using energy norm, H^2 norm, H^1 norm and L^2 norm. The calculations are carried out on the family of smoothly remapped hexagonal meshes.

These results show that optimal convergence rates are maintained by the VEM even for very sharp crack profiles, although the error constant increases, thus needing higher refinements to achieve a given solution accuracy.

7. Conclusions and final remark

In this work, we proposed a C^1 -regular virtual element method for the numerical approximation of a fourth-order phase-field equation. The virtual element formulation presented in this work employs a polynomial projection operator that combines the biharmonic and Laplace differential operators. We proved the convergence of the method and derived optimal convergence rates in different norms. The theoretical convergence results were confirmed by conducting numerical experiments on a set of four polygonal meshes. The good approximation properties of the proposed VEM are also demonstrated in the context of a problem involving HOPF representation of a crack.

Developing analogous discrete spaces and carrying out the *a priori* analyses for higher dimension model problems will be the topic of future research. Furthermore, coupling the HOPF evolution equation with the momentum balance equation forms the basis of HOPF models of dynamic fracture. With this in mind, in future work, we will be focusing our efforts on coupling the VEM that we recently developed for the momentum equation in [4] with the VEM presented herein.

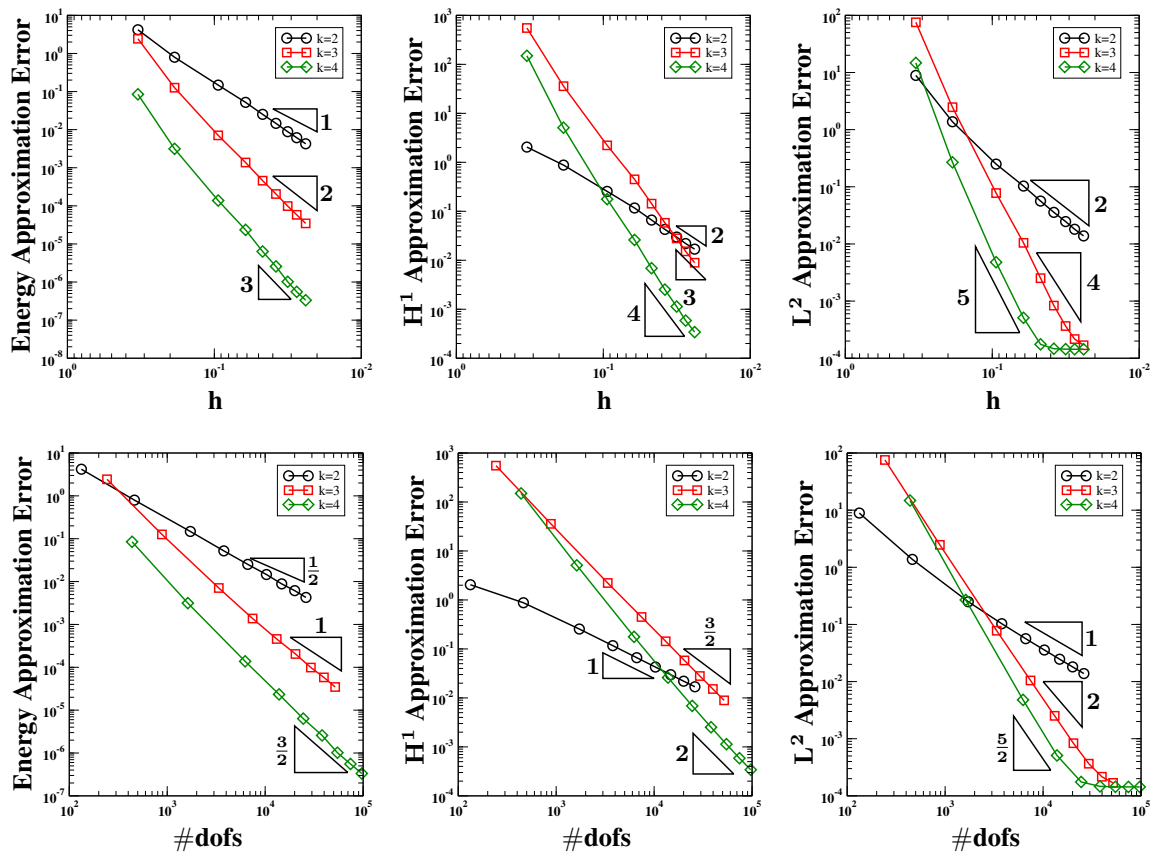


Figure 6: Test Case 1. Error curve measured using energy norm, H^2 norm, H^1 norm and L^2 norm. The calculations are carried out on the family of nonconvex octagonal meshes.

Acknowledgments

The authors gratefully acknowledge the support of the Laboratory Directed Research and Development (LDRD) program of Los Alamos National Laboratory under project number 20220129ER. Los Alamos National Laboratory is operated by Triad National Security, LLC, for the National Nuclear Security Administration of U.S. Department of Energy (Contract No. 89233218CNA000001). This work is registered as the Los Alamos Technical Report *LA-UR-21-31995*.

References

- [1] D. Adak, D. Mora, S. Natarajan, and A. Silgado. A virtual element discretization for the time dependent Navier–Stokes equations in stream-function formulation. *ESAIM: Math. Model. Numer. Anal.*, 55(5):2535–2566, 2021.
- [2] R. A. Adams and J. J. F. Fournier. *Sobolev spaces*. Pure and Applied Mathematics. Academic Press, 2 edition, 2003.
- [3] P. F. Antonietti, L. Beirão da Veiga, S. Scacchi, and M. Verani. A C^1 virtual element method for the Cahn-Hilliard equation with polygonal meshes. *SIAM J. Numer. Anal.*, 54(1):34–56, 2016.

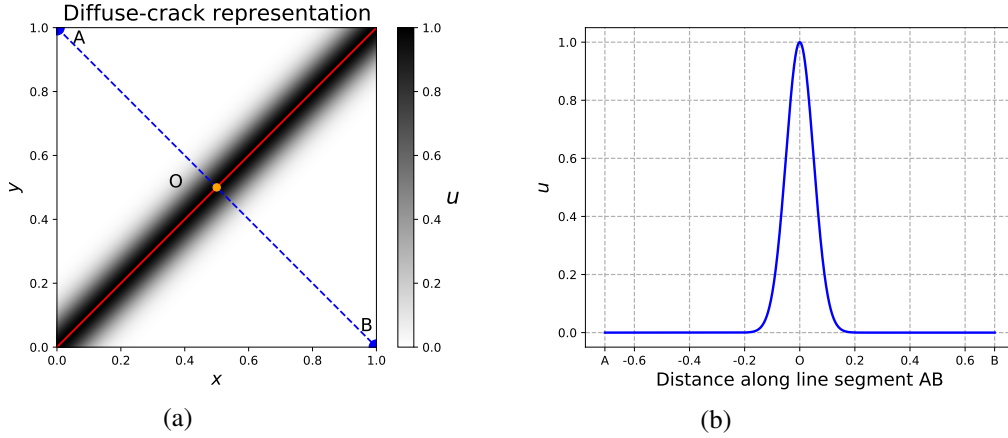


Figure 7: Test Case 2. A manufactured solution to HOPF equation. (a) Diffuse representation of a diagonal crack defined by the bisecting line $y = x$ (drawn in red color) and (b) PF profile along line segment AB for $\epsilon = 10^{-2}$.

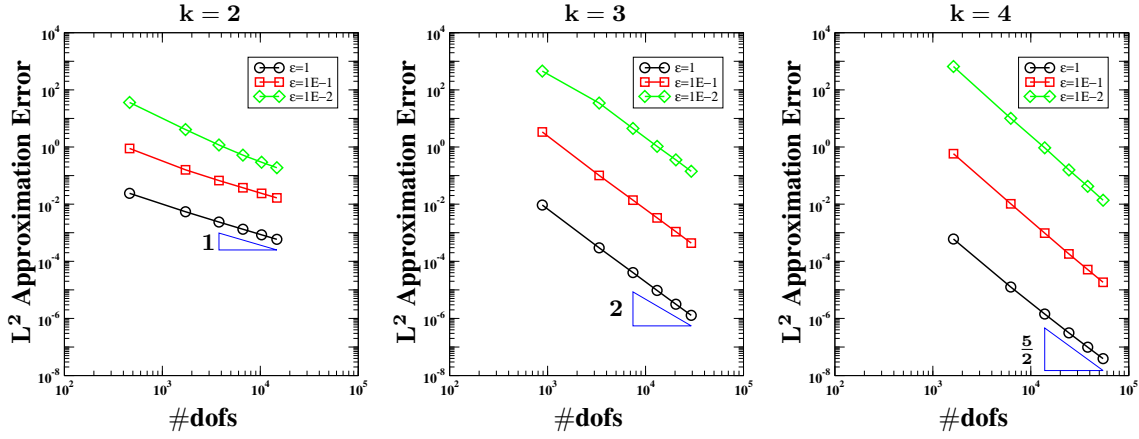


Figure 8: Test Case 2. Error curve measured using the L^2 norm for $\epsilon \in \{1, 10^{-1}, 10^{-2}\}$. The calculations are carried out on the family of randomized quadrilateral meshes using the virtual element method for $k = 2, 3, 4$.

- [4] P. F. Antonietti, G. Manzini, I. Mazzi, H.M. Mourad, and M. Verani. The arbitrary-order virtual element method for linear elastodynamics models: Convergence, stability and dispersion-dissipation analysis. *Internat. J. Numer. Methods Eng.*, 122:934–971, 2021.
- [5] P. F. Antonietti, G. Manzini, S. Scacchi, and M. Verani. A review on arbitrarily regular conforming virtual element methods for second- and higher-order elliptic partial differential equations. *Mathematical Models and Methods in Applied Sciences*, 31(14):2825 – 2853, 2021.
- [6] P. F. Antonietti, G. Manzini, and M. Verani. The conforming virtual element method for polyharmonic problems. *Comput. Math. Appl.*, 79(7):2021–2034, 2020.
- [7] J. H. Argyris, I. Fried, and D. W. Scharpf. The TUBA family of plate elements for the matrix displacement method. *Aeronaut. J. R. Aeronaut. Soc.*, 72:701–709, 1968.
- [8] B. Ayuso de Dios, K. Lipnikov, and G. Manzini. The non-conforming virtual element method. *ESAIM: Math. Model. Numer.*, 50(3):879–904, 2016.

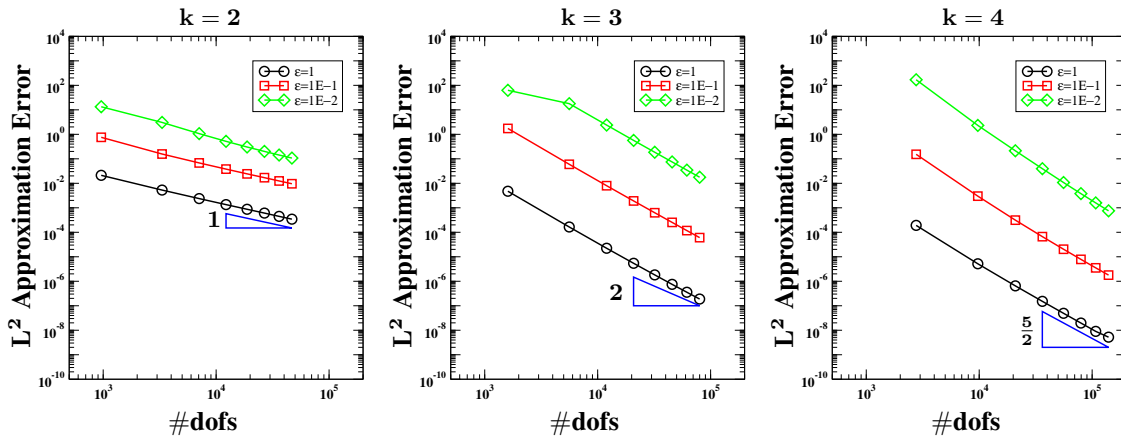


Figure 9: Test Case 2. Error curve measured using the L^2 norm for $\epsilon \in \{1, 10^{-1}, 10^{-2}\}$. The calculations are carried out on the family of smoothly remapped hexagonal meshes using the virtual element method for $k = 2, 3, 4$.

- [9] A. Bartezzaghi, L. Dedè, and A. Quarteroni. Isogeometric analysis of high order partial differential equations on surfaces. *Computer Methods in Applied Mechanics and Engineering*, 295:446–469, 2015.
- [10] L. Beirão da Veiga, F. Brezzi, A. Cangiani, G. Manzini, L. D. Marini, and A. Russo. Basic principles of virtual element methods. *Math. Models Methods Appl. Sci.*, 23(1):199–214, 2013.
- [11] L. Beirão da Veiga, F. Brezzi, L. D. Marini, and A. Russo. The hitchhiker’s guide to the virtual element method. *Math. Models Methods Appl. Sci.*, 24(8):1541–1573, 2014.
- [12] L. Beirão da Veiga and G. Manzini. A virtual element method with arbitrary regularity. *IMA J. Numer. Anal.*, 34(2):782–799, 2014.
- [13] L. Beirão da Veiga and G. Manzini. Residual *a posteriori* error estimation for the virtual element method for elliptic problems. *ESAIM: Math. Model. Numer. Anal.*, 49(2):577–599, 2015.
- [14] K. Bell. A refined triangular plate bending finite element. *Int. J. Numer. Meth. Eng.*, 1(1):101–122, 1969.
- [15] S. Berrone, A. Borio, and Manzini. SUPG stabilization for the nonconforming virtual element method for advection–diffusion–reaction equations. *Comput. Methods Appl. Mech. Eng.*, 340:500–529, 2018.
- [16] M. J. Borden, T. J. R. Hughes, C. M. Landis, and C. V. Verhoosel. A higher-order phase-field model for brittle fracture: Formulation and analysis within the isogeometric analysis framework. *Comput. Methods Appl. Mech. Eng.*, 273:100–118, 2014.
- [17] M. J. Borden, C. V. Verhoosel, M. A. Scott, T. J. R. Hughes, and C. M. Landis. A phase-field description of dynamic brittle fracture. *Comput. Methods Appl. Mech. Eng.*, 217:77–95, 2012.
- [18] B. Bourdin, G. A. Francfort, and J-J. Marigo. Numerical experiments in revisited brittle fracture. *J. Mech. Phys. Solids*, 48:797–826, 2000.
- [19] S. C. Brenner and R. Scott. *The mathematical theory of finite element methods*, volume 15. Springer Science & Business Media, 2008.

- [20] F. Brezzi and L. D. Marini. Virtual element methods for plate bending problems. *Comput. Methods Appl. Mech. Eng.*, 253:455–462, 2013.
- [21] C. Chen, X. Huang, and H. Wei. H^m -conforming virtual elements in arbitrary dimension. *SIAM Journal on Numerical Analysis*, 60(6):3099–3123, 2022.
- [22] C. Chinosi and L. D. Marini. Virtual element method for fourth order problems: L^2 -estimates. *Comput. Math. Appl.*, 72(8):1959–1967, 2016.
- [23] P. G. Ciarlet. *The Finite Element Method for Elliptic Problems*. Classics in Applied Mathematics. Society for Industrial and Applied Mathematics, 2002.
- [24] M. Dittmann, F. Aldakheel, J. Schulte, F. Schmidt, M. Krüger, P. Wriggers, and C. Hesch. Phase-field modeling of porous-ductile fracture in non-linear thermo-elasto-plastic solids. *Comput. Methods Appl. Mech. Eng.*, 361:112730, 2020.
- [25] A. Egger, U. Pillai, K. Agathos, E. Kakouris, E. Chatzi, I. A. Aschroft, and S. P. Triantafyllou. Discrete and phase field methods for linear elastic fracture mechanics: A comparative study and state-of-the-art review. *Appl. Sci.*, 9(12):2436, 2019.
- [26] C. M. Elliott, D. A. French, and F. A. Milner. A second-order splitting method for the Cahn-Hilliard equation. *Numer. Math.*, 54(5):575–590, 1989.
- [27] G. A. Francfort and J. J. Marigo. Revisiting brittle fracture as an energy minimization problem. *J. Mech. Phys. Solids*, 46:1319–1342, 1998.
- [28] E. H. Georgoulis and P. Houston. Discontinuous Galerkin methods for the biharmonic problem. *IMA J. Numer. Anal.*, 29(3):573–594, 2009.
- [29] S. Goswami, C. Anitescu, and T. Rabczuk. Adaptive fourth-order phase field analysis using deep energy minimization. *Theor. Appl. Fract. Mech.*, 107:102527, 2020.
- [30] P. Grisvard. *Elliptic problems in nonsmooth domains*, volume 24 of *Monographs and Studies in Mathematics*. Pitman (Advanced Publishing Program), Boston, MA, 1985.
- [31] P. Grisvard. *Singularities in boundary value problems and exact controllability of hyperbolic systems*. Springer, 1992.
- [32] J. Hu, T. Lin, and Q. Wu. A construction of C^r conforming finite element spaces in any dimension. Preprint arXiv:2103.14924, 2021.
- [33] R. Ma and W.C. Sun. FFT-based solver for higher-order and multi-phase-field fracture models applied to strongly anisotropic brittle materials. *Comput. Methods Appl. Mech. Eng.*, 362:112781, 2020.
- [34] C. Miehe, M. Hofacker, L. M. Schänzel, and F. Aldakheel. Phase field modeling of fracture in multi-physics problems. Part II. Coupled brittle-to-ductile failure criteria and crack propagation in thermo-elastic-plastic solids. *Comput. Methods Appl. Mech. Eng.*, 294:486–522, 2015.
- [35] C. Miehe, F. Welschinger, and M. Hofacker. Thermodynamically consistent phase-field models of fracture: Variational principles and multi-field FE implementations. *Int. J. Numer. Methods Eng.*, 83(10):1273–1311, 2010.
- [36] G. Moutsanidis, D. Kamensky, J. S. Chen, and Y. Bazilevs. Hyperbolic phase field modeling of brittle fracture: Part II—immersed IGA–RKPM coupling for air-blast–structure interaction. *J. Mech. Phys. Solids*, 121:114–132, 2018.

- [37] M. N. Rahimi and G. Moutsanidis. Modeling dynamic brittle fracture in functionally graded materials using hyperbolic phase field and smoothed particle hydrodynamics. *Comput. Methods Appl. Mech. Eng.*, 401:115642, 2022.
- [38] S. Rezaei, A. Harandi, T. Brepols, and S. Reese. An anisotropic cohesive fracture model: Advantages and limitations of length-scale insensitive phase-field damage models. *Eng. Fract. Mech.*, 261:108177, 2022.
- [39] R. H. Stogner, G. F. Carey, and B. T. Murray. Approximation of Cahn–Hilliard diffuse interface models using parallel adaptive mesh refinement and coarsening with C^1 elements. *Int. J. Numer. Methods Eng.*, 76(5):636–661, 2008.
- [40] G. Strang. Variational crimes in the finite element method. In *The Mathematical Foundations of the Finite Element Method with Applications to Partial Differential Equations*, pages 689–710. Elsevier, 1972.
- [41] L. Svolos, C. A. Bronkhorst, and H. Waisman. Thermal-conductivity degradation across cracks in coupled thermo-mechanical systems modeled by the phase-field fracture method. *J. Mech. Phys. Solids*, 137:103861, 2020.
- [42] L. Svolos, H. M. Mourad, C. A. Bronkhorst, and H. Waisman. Anisotropic thermal-conductivity degradation in the phase-field method accounting for crack directionality. *Eng. Fract. Mech.*, 245:107554, 2021.
- [43] L. Svolos, H.M. Mourad, G. Manzini, and K. Garikipati. A fourth-order phase-field fracture model: Formulation and numerical solution using a continuous/discontinuous Galerkin method. *J. Mech. Phys. Solids*, 165:104910, 2022.
- [44] J. Vignollet, S. May, R. De Borst, and C.V. Verhoosel. Phase-field models for brittle and cohesive fracture. *Meccanica*, 49(11):2587–2601, 2014.
- [45] J.-Y. Wu, V. P. Nguyen, C. T. Nguyen, D. Sutula, S. Sinaie, and S. P. A. Bordas. Chapter One - Phase-field modeling of fracture. In Stéphane P. A. Bordas and Daniel S. Balint, editors, *Advances in Applied Mechanics*, volume 53, pages 1–183. Elsevier, 2020.
- [46] C. Yan, X. Wang, D. Huang, and G. Wang. A new 3D continuous-discontinuous heat conduction model and coupled thermomechanical model for simulating the thermal cracking of brittle materials. *Int. J. Solids Struct.*, 229:111123, 2021.
- [47] S. Zhang. A family of differentiable finite elements on simplicial grids in four space dimensions. *Math. Numer. Sin.*, 38(3):309–324, 2016.

Statements & Declarations

Funding.: Laboratory Directed Research and Development (LDRD) program operated at Los Alamos National Laboratory, Grant N. 20220129ER

Competing Interests.: All the Authors have no financial interests.

Author Contributions.: All the Authors equally contributed to this work.

Data Availability.: No new data were specifically generated for this work. The meshes utilized for this study and reported in the final appendix are the property of Los Alamos National Laboratory and can be made available on reasonable request.

Appendix A. Mesh data

For completeness, we report the data corresponding to the four mesh families that we used in the calculation of Section sec6:numerical:results. The four tables report the following data:

- n : refinement level;
- N_P, N_F, N_V : number of elements, edges, and vertices;
- h : mesh size parameter;
- $\#\text{dofs}_{k=\ell}$: total number of degrees of freedom for the VEM with polynomial degree $\ell = 2, 3, 4$.

n	N_P	N_F	N_V	h	$\#\text{dofs}_{k=2}$	$\#\text{dofs}_{k=3}$	$\#\text{dofs}_{k=4}$
0	25	60	36	$3.788 \cdot 10^{-1}$	133	243	438
1	100	220	121	$2.007 \cdot 10^{-1}$	463	883	1623
2	400	840	441	$1.035 \cdot 10^{-1}$	1723	3363	6243
3	900	1860	961	$6.907 \cdot 10^{-2}$	3783	7443	13863
4	1600	3280	1681	$5.195 \cdot 10^{-2}$	6643	13123	24483
5	2500	5100	2601	$4.155 \cdot 10^{-2}$	10303	20403	38103
6	3600	7320	3721	$3.466 \cdot 10^{-2}$	14763	29283	54723
7	4900	9940	5041	$2.970 \cdot 10^{-2}$	20023	39763	74343
8	6400	12960	6561	$2.600 \cdot 10^{-2}$	26083	51843	96963

Table A.1: Mesh data and number of degrees of freedom for the VEM with polynomial degree $k = 2, 3, 4$ for the family of smoothly remapped quadrilateral meshes.

n	N_P	N_F	N_V	h	$\#\text{dofs}_{k=2}$	$\#\text{dofs}_{k=3}$	$\#\text{dofs}_{k=4}$
0	25	60	36	$3.311 \cdot 10^{-1}$	133	243	438
1	100	220	121	$1.865 \cdot 10^{-1}$	463	883	1623
2	400	840	441	$9.412 \cdot 10^{-2}$	1723	3363	6243
3	900	1860	961	$6.130 \cdot 10^{-2}$	3783	7443	13863
4	1600	3280	1681	$4.693 \cdot 10^{-2}$	6643	13123	24483
5	2500	5100	2601	$3.808 \cdot 10^{-2}$	10303	20403	38103
6	3600	7320	3721	$3.167 \cdot 10^{-2}$	14763	29283	54723
7	4900	9940	5041	$2.751 \cdot 10^{-2}$	20023	39763	74343
8	6400	12960	6561	$2.389 \cdot 10^{-2}$	26083	51843	96963

Table A.2: Mesh data and number of degrees of freedom for the VEM with polynomial degree $k = 2, 3, 4$ for the family of randomized quadrilateral meshes.

n	N_P	N_F	N_V	h	#dofs $_{k=2}$	#dofs $_{k=3}$	#dofs $_{k=4}$
0	36	125	90	$3.279 \cdot 10^{-1}$	306	503	861
1	121	400	280	$1.846 \cdot 10^{-1}$	961	1603	2766
2	441	1400	960	$9.686 \cdot 10^{-2}$	3321	5603	9726
3	961	3000	2040	$6.492 \cdot 10^{-2}$	7081	12003	20886
4	1681	5200	3520	$4.889 \cdot 10^{-2}$	12241	20803	36246
5	2601	8000	5400	$3.914 \cdot 10^{-2}$	18801	32003	55806
6	3721	11400	7680	$3.265 \cdot 10^{-2}$	26761	45603	79566
7	5041	15400	10360	$2.799 \cdot 10^{-2}$	36121	61603	107526
8	6561	20000	13440	$2.451 \cdot 10^{-2}$	46881	80003	139686

Table A.3: Mesh data and number of degrees of freedom for the VEM with polynomial degree $k = 2, 3, 4$ for the family of smoothly remapped hexagons.

n	N_P	N_F	N_V	h	#dofs $_{k=2}$	#dofs $_{k=3}$	#dofs $_{k=4}$
0	25	120	96	$2.915 \cdot 10^{-1}$	313	483	798
1	100	440	341	$1.458 \cdot 10^{-1}$	1123	1763	2943
2	400	1680	1281	$7.289 \cdot 10^{-2}$	4243	6723	11283
3	900	3720	2821	$4.859 \cdot 10^{-2}$	9363	14883	25023
4	1600	6560	4961	$3.644 \cdot 10^{-2}$	16483	26243	44163
5	2500	10200	7701	$2.915 \cdot 10^{-2}$	25603	40803	68703
6	3600	14640	11041	$2.430 \cdot 10^{-2}$	36723	58563	98643
7	4900	19880	14981	$2.082 \cdot 10^{-2}$	49843	79523	133983
8	6400	25920	19521	$1.822 \cdot 10^{-2}$	64963	103683	174723

Table A.4: Mesh data and number of degrees of freedom for the VEM with polynomial degree $k = 2, 3, 4$ for the family of nonconvex octagons.